GOLD NANOSPHERE-THIOCTIC ACID-Zn(SALOPHEN) CONJUGATE: SYNTHESIS, CHARACTERISATION, TOXICITY AND PROTEIN INTERACTION

NG YIN ZHUANG

FACULTY OF SCIENCE
UNIVERSITI MALAYA
KUALA LUMPUR

2022

GOLD NANOSPHERE-THIOCTIC ACID-Zn(SALOPHEN) CONJUGATE: SYNTHESIS, CHARACTERISATION, TOXICITY AND PROTEIN INTERACTION

NG YIN ZHUANG

DISSERTATION SUBMITTED IN FULFILMENT OF THE REQUIREMENTS FOR THE DEGREE OF MASTER OF SCIENCE

FACULTY OF SCIENCE
UNIVERSITI MALAYA
KUALA LUMPUR

2022

UNIVERSITI MALAYA
ORIGINAL LITERARY WORK DECLARATION

Name of Candidate: **NG YIN ZHUANG**

Matric No: **17028390/2**

Name of Degree: **MASTER OF SCIENCE**

Title of Dissertation ("this Work"):

GOLD NANOSPHERE-THIOCTIC ACID-Zn(SALOPHEN) CONJUGATE: SYNTHESIS, CHARACTERISATION, TOXICITY AND PROTEIN INTERACTION

Field of Study:

INORGANIC CHEMISTRY

I do solemnly and sincerely declare that:

(1) I am the sole author/writer of this Work;
(2) This Work is original;
(3) Any use of any work in which copyright exists was done by way of fair dealing and for permitted purposes and any excerpt or extract from, or reference to or reproduction of any copyright work has been disclosed expressly and sufficiently and the title of the Work and its authorship have been acknowledged in this Work;
(4) I do not have any actual knowledge nor do I ought reasonably to know that the making of this work constitutes an infringement of any copyright work;
(5) I hereby assign all and every rights in the copyright to this Work to the University of Malaya ("UM"), who henceforth shall be owner of the copyright in this Work and that any reproduction or use in any form or by any means whatsoever is prohibited without the written consent of UM having been first had and obtained;
(6) I am fully aware that if in the course of making this Work I have infringed any copyright whether intentionally or otherwise, I may be subject to legal action or any other action as may be determined by UM.

Candidate's Signature Date: 27/6/2022

Subscribed and solemnly declared before,

Witness's Signature Date:27/6/22

Name:

Designation:

GOLD NANOSPHERE-THIOCTIC ACID-Zn(SALOPHEN) CONJUGATE: SYNTHESIS, CHARACTERISATION, TOXICITY AND PROTEIN INTERACTION

ABSTRACT

A novel inorganic metal complex gold nanoparticle conjugate was synthesised and characterised in this study. It was achieved by conjugating a Schiff base zinc complex, [N,N-bis(salicylidene)-1,2-phenylenediamine]zinc(II) or commonly known as Zn(salophen) (ZnS) to gold nanosphere with thioctic acid functioning as the linker. The conjugate (AuNS-TA-ZnS) was characterised with FTIR, UV-visible spectroscopy, fluorescence spectroscopy, dynamic light scattering (DLS) analysis, zeta potential analysis, inductively coupled plasma mass spectrometry (ICP-MS) analysis and transmission electron microscope (TEM). Both AuNS-TA-ZnS and ZnS were confirmed to be the proposed structures. The diameter of AuNS-TA-ZnS was determined to be 17.73 nm with 1785 ZnS conjugated to each gold nanosphere. The interactions of AuNS-TA-ZnS with proteins were studied. It was found that the conjugate has strong affinity to Bovine Serum Albumin (BSA). AuNS-TA-ZnS is able to alter the secondary structure of BSA without causing conformational change to the tertiary structure of BSA. Apart from demonstrating the ability to generate reactive oxygen species (ROS), AuNS-TA-ZnS also inhibits proteasome activities specifically at the Trypsin-like site of mouse 20S proteasome. Cytotoxicity study with breast cancer cells shows that AuNS-Ta-ZnS is more cytotoxic than unconjugated ZnS. Transepithelial electrical resistance (TEER) measurement across Caco-2 cell monolayer found AuNS-TA-ZnS has higher efficiency than ZnS in permeating thru the cells.

Keywords: gold nanosphere, conjugate, Zn(salophen), protein interaction, cytotoxic

KONJUGASI NANOSFERA EMAS-ASID THIOCTIC-Zn(SALOPHEN): SINTESIS, PENCIRIAN, KETOSIKAN DAN INTERAKSI PROTEIN

ABSTRAK

Dalam kajian ini, satu konjugasi baru antara komplex inorganik dan nanosfera emas telah disintesis dan ciri-cirinya dikaji. Komplex zink bes Schiff, [N,N-bis(salisilikena)-1,2-fenilenadiamina] zink(II) atau lebih dikenali sebagai Zn(salophen) (ZnS) dikonjugasikan ke nanosfera emas dengan mengunakan asid tiotik sebagai media penghubung. Ciri-ciri AunNS-TA-ZnS telah dikaji dengan FTIR, spektroskopi sinar ultra-ungu-dilihat (UV-visible), spektroscopi pendarflour, analisis penyebaran cahaya dinamik (DLS), analisis potensi zeta, analysis spektroskopi jisim plasma berganding induktif (ICP-MS) dan mikroskop electron penghantaran (TEM). Hasil analis mengesahkan bahawa struktur AuNS-TA-ZnS dan ZnS adalah seiras dengan struktur yang dicadangkan. Diameter AuNS-TA-ZnS diukur sepanjang 17.73 nm dan sebanyak 1785 komplex ZnS dijumpai bagi setiap nonosfera emas. Interaksi AuNS-TA-ZnS dengan protein turut dikaji dan didapati bahawa AuNS-TA-ZnS mempunyai pertalian yang kuat terhadap albumin serum lembu (BSA). AuNS-TA-ZnS boleh mengubah stuktur sekunder BSA tanpa mengubah konformasi tertiari BSA. AuNS-TA-ZnS mampu menghasilkan spesies oksigen reaktif (ROS) dan menghalang aktiviti proteasome terutamanya di tapak Trypsin-like 20S proteasome tikus. Kajian sitotoksik dengan sel-sel barah payudara menunjukkan AuNS-TA-ZnS lebih sitotoksik berbanding dengan ZnS. Bacaan rintagan elektrik trasnsepithelial (TEER) ke atas lapisan tunggal sel Caco-2 mendapati bahawa AuNS-TA-ZnS mempunyai kebolehtelapan yang lebih tinggi daripada ZnS.

Kata kunci: Nanosfera emas, konjugasi, Zn(salophen), interaksi protein, sitotosiksiti

ACKNOWLEDGEMENTS

I would like to thank my family for giving their continuous support and understanding throughout this journey. My deepest appreciation also goes to my supervisor Dr Ng Chew Hee and Dr. Tan Kong Wai. Thank you for giving me the opportunity to carry out this research, provided me with guidance and offered valuable insights which helped me to see things from different perspective.

Not to forget my peers, Dr. Yap Yiing Jye, Ms. Ng Pei Ying, Ms. Lai Jing Wei, Ms. Chan Cheang Wei and Dr. Low May Lee. Along with their presences, they also bought me lots of encouragements, sharing, and offers which motivate me to move forward.

Besides, a million thanks to the lab staffs in International Medical University's research lab, namely Ms. Nor Bazlin, Ms. Malathi, Ms. Siew Lye Kuan, Ms. Yong Lee Mei, Ms. Norsoleha and Ms. Diana who were always generous in offering technical support. I am also very grateful for the technical support offered by Mr. Amir when I was using TEM in the University Malaya Physics Department.

Last but not least, thank you to Ministry of Higher Education for funding this research thru the Fundamental Research Grant Scheme (FRGS/2/2014/ST01/IMU/02/1).

TABLE OF CONTENTS

LIST OF FIGURES

LIST OF TABLES

LIST OF SYMBOLS AND ABBREVIATIONS

ϵ	:	Molar absorptivity
AMC	:	7-amino-4-methylcoumarin
ATCC	:	American type culture collection
ATR	:	Attenuated total reflectance
AuNS	:	Gold nanosphere
AuNS-TA	:	Gold nanosphere-thioctic acid
AuNS-TA-ZnS	:	Gold nanosphere-thioctic acid-zn(salophen)
Boc	:	t-Butyloxycarbonyl
BSA	:	Bovine serum albumin
C-L	:	Caspase-like
CT-L	:	Chymotrypsin-like
Caco-2	:	Human colon cancer
CD	:	Circular dichroism
CHN	:	Carbon, hydrogen and nitrogen
DCFH-DA	:	Dichlorofluorescin diacetate
DLS	:	Dynamic light scattering
DMEM	:	Dulbecco's modified eagle medium
DNA	:	Deoxyribonucleic acid
EPR	:	Enhanced permeability and retention
FBS	:	Fetal bovine serum
FTIR	:	Fourier transform infrared
Glu	:	Glutamic acid
GNP	:	Gold nanoparticles
HBSS	:	Hank's buffer salt solution

HCl	:	Hydrochloric acid
ICP-MS	:	Inductively coupled plasma mass spectroscopic
IC_{50}	:	50% growth inhibition
IgG	:	Immune-globulin
Leu	:	Leucine
MCF-7	:	Human breast cancer
MDA-MB-231	:	Human breast cancer
MDA-MB-468	:	Human breast cancer
MEF	:	Metal enhanced fluorescence
MLCT	:	Metal ligand charge transfer
M-O	:	Metal-oxygen
MTT	:	3-(4,5-dimethylthiazol-2-yl)-2,5 diphenyl tetrazolium bromide
PBS	:	Phosphate buffer solution
PCR	:	Polymerase chain reaction
Phe	:	Phenylalanine
ROS	:	Reactive oxygen species
RNA	:	Ribonucleic acid
SPR	:	Surface plasmon resonance
Suc	:	N-succinyl
T-L	:	Trypsin-like
TA	:	Thioctic acid
TEER	:	Transepithelial electrical resistance
TEM	:	Transmission electron microscopy
Trp	:	Tryptophan
Tyr	:	Tyrosine
UV-Vis	:	Ultraviolet-visible

Val	:	Valine
Z	:	Benzyloxycarbonyl
ZnS	:	Zinc(II) salophen

CHAPTER 1: INTRODUCTION

Nanoparticles are gaining much attention lately. The usage of gold nanoparticles (GNP) in medical field is being welcomed due to its robustness in synthesis and surface modification, high stability and biologically inert.

With its large surface area to volume ratio, GNP could be surface-functionalised with various molecules. This modification will alter the properties of these GNP, leading to multitude applications (Erik C. Dreaden et al., 2011; Egea et al., 2019). Although there are numerous different types of GNP conjugates; conjugates of inorganic metal complex to GNP do not get much attention.

Since metal complexes have its own tuneable characteristic properties, conjugates of metal complex to GNP are forming an emerging subclass of interesting nanoparticles consisting of a gold core with an outer shell of metal-containing structures (Dumur et al., 2020). As far as we are concerned, there are few GNP-metal complex conjugates being reported (Beloglazkina et al., 2012).

There is a continuous need to investigate the toxicity of nanoparticles as their popularity has caused both human and organisms to be exposed by these nanoparticles more frequently (Jeevanandam et al., 2018). Although GNP are useful for biological applications, however there are conflicting reports on their toxicity (Ellen E Connor et al., 2005; N. Khlebtsov et al., 2011).

Besides, it is also crucial for us to understand how our biological system will response when it is exposed to nanoparticles and interacted with proteins (Dasgupta et al., 2016; Dell'Orco et al., 2014). Factors such as size, shape and charge are known to be affecting the permeability and cellular uptake of GNP (Carnovale et al., 2016). Moreover, the

conformation of proteins is important to their biological activities. Interaction of proteins with GNP might alter the conformation of proteins to varying degree (Lynch et al., 2008).

In this study, an attempt was made to synthesise an inorganic gold nanosphere conjugated with metal complex. The gold nanosphere (AuNS) was synthesised by using Turkevich method with citrate ions as the reducing agent to obtain gold nanosphere with diameter around 14 nm. The citrate ions of the citrate capped gold nanosphere was then removed and replaced with thioctate ions as Au-S bonds were known to be stronger.

Conjugation of zinc Schiff base complex, [N,N'-bis(salicylidene)-1,2-phenylenediamine]zinc(II) or more widely known as zinc(II) salophen (ZnS) with gold nanosphere was then carried out to obtain the conjugate, AuNS-TA-ZnS. Herein, this dissertation also reported the characterisation of AuNS-TA-ZnS, its toxicity, cell membrane permeability and interaction with BSA and proteasome.

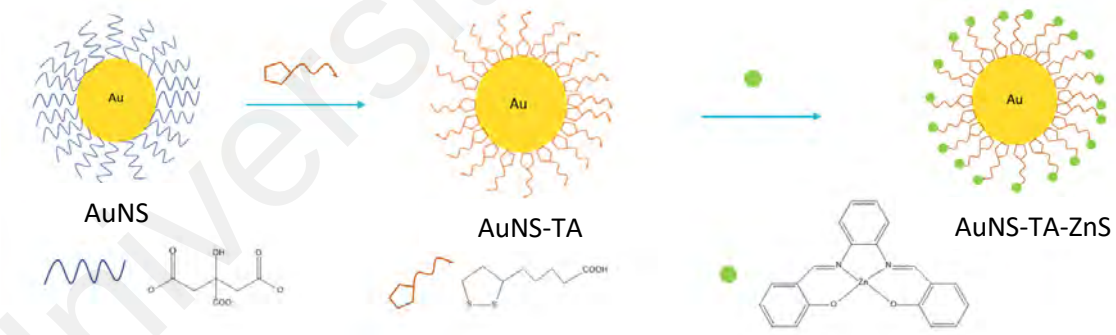

Figure 1.1: Synthetic scheme of AuNS-TA-ZnS.

The objectives of this study are

(i) To synthesise and characterise AuNS-TA-ZnS.

(ii) To investigate the cytotoxicity and permeability of AuNS-TA-ZnS.

(iii) To investigate the interaction of AuNS-TA-ZnS with 20S proteasome and BSA.

There is a total of 5 chapters in this dissertation. Chapter 2 presents the literature reviews of GNP conjugates, Schiff base and their metal complexes, toxicity and protein interaction. Chapter 3 outlines the experimental method of this study. Chapter 4 will be the presentation of the results obtained and its discussion. Chapter 5 concludes the study and offers suggestions for future works.

CHAPTER 2: LITERATURE REVIEW

2.1 Gold Nanoparticles (GNP) Conjugates

GNP are a cluster of gold atoms clumping together to form a particle with its size ranging from 1- 100 nm (Alanazi et al., 2010). The usage of GNP could be traced back to the Roman empire where a glass product named Lycurgus cup was made. It gives different colours when light is shine from different angles due to the present of GNP. (Slepička et al., 2019). During the Renaissance era, GNP were used to made ruby coloured glass. It was until latter, discovery found that the ability to project ruby colour is due to a phenomenon named surface plasmon resonance (SPR) effect.

Unlike bulk gold, GNP own new and different set of properties due to its nano size which makes surface property becomes a dominant property (Xiaohua Huang et al., 2006). Surface of GNP are covered with free electrons in the conduction bands (Maier, 2007). When induced by light waves which have frequency in resonance with the oscillations of these free electrons, the electrons oscillate coherently causing the SPR effect (Amendola et al., 2017). This generates strong electric field at the surface of GNP. This unique property makes GNP an efficient catalyst in organic reactions such as oxidation of alcohol (Alanazi et al., 2010; Hu et al., 2007), increase the efficiency of polymerase chain reaction (PCR) (Huang et al., 2008) and sensors to detect tumour markers (Fu, 2007; Zhuo et al., 2005).

The effect of SPR could be tuned as it is under the influence of the size, shape, surface charge and surrounding environment of the GNP (Navarrete et al., 2018). Fortunately, the size, shape and surface charge of GNP can be manipulated via different synthesis methods, with all the methods working under the same principle: reduction of gold(III) or gold(I) ions to gold atom.

GNP with different surfaces could be synthesis by using different methods as reported by literatures. One of the widely used protocol is Turkevich method which uses citrate ions as the reducing agent to yield gold nanosphere capped with citrate (Turkevich et al., 1951); Burst-Schiff method that produces hydrophobic gold nanosphere (Brust et al., 1994) and electrochemical method which reduced gold ions to nanoparticles at the electrode (Reetz et al., 1994). Apart from gold nanosphere, we could also get GNP in other shapes by using seeding growth method that produce gold nanorod (Jana et al., 2001) or green synthesis method with reduction drives by plant extract to give shapes like nanotriangle and nanorod (Arunachalam et al., 2013; Chandran et al., 2006; Shankar et al., 2004; Sujitha et al., 2013).

As scientists are in keen search on non-invasive technique to treat various diseases which at the same time would only bring minimal impact to the normal cells, GNP appear to be a suitable candidate. Owning to its large surface area to volume ratio and their surface could be engineered to bind with other molecules, this led us to the research on GNP conjugates.

2.1.1 GNP-Antibody Conjugate

GNP conjugated with antibody are studied widely. In immunohistochemistry, GNP-antibody conjugate is used as sensor electrode to detect antibody-antigen interaction (Wang et al., 2004). In the attempts of obtaining the balance between having more receptor binding sites versus avoiding inefficient endocytosis due to large particle size, the robustness of synthesizing GNP in different sizes becomes helpful. Eventually, Jiang et al. (2008) found that GNP conjugated with immune-globulin (IgG) antibody in the size of 40-50 nm would be suitable.

Upon conjugation with antibody, the antibody on the GNP-antibody conjugates could carry out targeted deliver of GNP to targeted site for photothermal therapy (X.

Huang et al., 2006; Pitsillides et al., 2003). Upon reaching the targeted site, strong electric field at the surface of GNP improve the effectiveness in converting the radiation illuminated from laser into heat (X. Huang et al., 2006). The increment of temperature in cells will disrupt their usual cellular function such as denature of enzymes, metabolic signalling disruption and inhibited nucleotide synthesis which eventually lead to cell death (E. C. Dreaden et al., 2011).

2.1.2 GNP-DNA / GNP-RNA Conjugate

Lately, gene therapy has a promising future in curing disease by treating it at the molecular level (Duarte et al., 2012). One of the potential candidates to deliver DNA or RNA for gene therapy is the GNP-DNA or GNP-RNA conjugates (Bonoiu et al., 2009). In cancer treatment with gene therapy, one of the techniques employed is gene silencing where RNA is used to silence genes that initiate tumour growth and spreading (Deng et al., 2014; Fujita et al., 2015). Unfortunately, there was few setbacks while delivering these free RNA, mainly due to their short lifetime and degradation by the circulating enzymes (R. Mendes et al., 2017). The challenges could be overcome by conjugating DNA or RNA with GNP. As GNP have higher molecular weight, it is able to achieve the enhanced permeability and retention (EPR) effect. This helps the GNP conjugates to accumulate at the vicinity of tumour, thus prolonging their retention duration (Maheshwari et al., 2019; Sandoval et al., 2019).

2.1.3 GNP-Organic Molecule Conjugate

Apart from the two types of GNP conjugates mentioned above; GNP could also conjugate with organic molecules such as doxorubicin, chloroquine, ciproflaxin, tamoxifen and curcumin (Cui et al., 2017). Upon conjugation, GNP act as drug delivery vehicles for the delivery of these organic molecules. Vigderman et al. (2013) reported that conjugates have higher toxicity than its free drugs, partly due to the EPR effect

mentioned above. Besides, the solubility of Paclitaxel, an organic molecule for chemotherapy was enhanced after conjugating with GNP which eventually increased its cytotoxicity (X.-Q. Zhang et al., 2011). Betulin, an anti-inflammatory drug has also overcome the same restriction thru forming conjugates with GNP. Mioc et al. (2018) reported that the solubility enhancement increased the bioavaibility of Betulin and boosted its therapeutic effect.

2.1.4 GNP-Metal Complex Conjugate

For inorganic metal complexes like Cisplatin, Min et al. (2010) found that its cytotoxicity was enhanced upon forming conjugates with GNP. It was explained as the cells could consume the conjugates easier via endocytosis when compared to the free Cisplatin. Most of the researches related to GNP-metal complex conjugates themed around platinum-based GNP conjugates (Craig et al., 2012; England et al., 2015; Ling et al., 2018; Parker et al., 2015) with other metal complexes received less attention. At this moment, there are few ruthenium-based GNP conjugates which were synthesized to function as bioimaging or photothermal agent (N. J. Rogers et al., 2014; P. Zhang et al., 2017; P. Zhang et al., 2015); a copper-based GNP conjugate serves as anticancer drug (Pramanik et al., 2016) while Vitale et al. (2008) successfully synthesized a palladium-based GNP conjugates. Researches on zinc-based GNP are mostly focusing on enhancing the photosenstitizer ability of zinc phthalocyanine and zinc porphyrins (Dube et al., 2018; Liang et al., 2019; Matlou et al., 2018; Mthethwa et al., 2013; Satake et al., 2009). Thus, with GNP carrying various unique properties that would alter the properties of metal complexes upon conjugation, GNP-metal complex conjugates have given us a huge space to discover more.

2.2 Schiff base

Salophen is a Schiff base ligand, one of the oldest ligands discovered in 1933 (Leoni et al., 2018). It can act as a tetradentate ligand with its 2 nitrogen atoms and 2 oxygen atoms. Due to the ease in synthesis and modification of salophen and its derivative, they are often coordinated to metal ions to form metal salophen complexes and be used extensively as catalyst for organic reactions such as synthesis of cyclic carbonate (Decortes et al., 2010), oxidation of alcohols (Bahramian et al., 2006), oxygenation of heteroatoms (Venkataramanan et al., 2005), azrinidation reaction (Omura et al., 2004) and Diels-Alder reaction (Antonella Dalla Cort et al., 2005). The researches on metal salophen and its derivatives keep progressing. In 2004, 1-phenyl-1-propanol was synthesised by Maeda et al. with a chiral zinc salophen as the asymmetric catalyst for the addition of diethylzinc to aldehydes. Another asymmetric catalyse for the epoxidation of olefins was also made possible with manganese salen derivatives (Katsuki, 1996). In 2010, Haak et al. reported various bimetallic salophen complexes as catalysts which performed more efficiently and selectively due to the simultaneous presence of Lewis acid and Lewis base in the same structure.

Besides, Schiff base complexes are also applied as sensors. Mirzaei et al. (2015) used Schiff base to detect the presence of aluminium and cadmium via potentiometric method. In the other hand, Ganjali et al. (2004) found that cobalt(II) salophen is able to detect nitrite ions while Abdel-Haleem et al., 2016 shows that Schiff base complex of manganese(III) and manganate(IV) could detect the presence of thiocyanate.

For biological applications of Schiff base metal complexes, nickel salophen (Lecarme et al., 2014) and platinum salophen derivatives (Wu et al., 2009) are able to bind and stabilize the G-quadruplex DNA structure, thus inhibit telomerase activities and cause cell death. Liu et al. (1994) found that manganese salen exhibits superoxide scavenging

activity; while Abdel-Haleem et al. (2016) discovered antibacterial property in gallium salophen.

2.3 Zinc(II) Salophen (ZnS)

The choice of metal ion in this study is zinc(II) ion due to its high abundancy in organism and its biocompatibility. They are highly bioavailable as metalloenzymes, where their flexibility in coordination geometry could aid the protein to carry out conformation changes in biological reactions.

ZnS has a five coordinated square planar geometry with the Schiff base, salophen taking the basal plane while the apical position is left to the solvent which can be replaced with ease by another group. This phenomenon is due to the high Lewis acidity at the metal centre of ZnS and which enable ZnS to function as fluorescence probe of inorganic phosphates (Cano et al., 2009) and amines (I. P. Oliveri et al., 2011).

Unfortunately, ZnS suffers from low solubility in water, thus limits their biological application. A. Dalla Cort et al. (2009) tried to overcome this difficulty by synthesizing a new ZnS derivative by attaching D-glucose at the 5,50 positions. Another attempt was made by Asadi et al. (2017) by conjugating lipophilic cation to the Schiff base ligand of the metal complex.

2.4 Toxicity

Toxicity of a drug was usually evaluated via in vitro cytotoxicity study, follow by in vivo animal testing before entering clinical trial on human (Lipsky et al., 2001). Cytotoxicity study is an economical way to determine the toxicity of a drug on cells for further evaluation of their anticancer potential (Garle et al., 1994). Besides, it is useful in predicting the acute toxicity for in vivo study, thus reduces the number of animals used for in vivo testing (Halle, 2003).

2.4.1 Toxicity of Metal(salophen)

It was learned that metal(salophen) exhibits different cytotoxicity level when salophen was coordinated to different metal ions. Routier et al. (1999) found that iron(III) salophen is able to generate reactive oxygen species via redox reaction of iron; and Lange et al. (2008) reported that iron(III) salophen could induce cell death and prevent cell proliferation on ovarian cancer. Derivatives of platinum(II) salophen are able to stabilize G-quadruplex DNA which eventually lead to cell death (Wu et al., 2009). Cytotoxicity studies show cobalt(III) salophen, nickel(II) salophen, derivatives of uranium(VI) salophen, oxovanadium(V) salophen are cytotoxic and posse potential to be anticancer drugs (Ambika et al., 2019,Rani et al., 2021, Ebrahimipour et al., 2017; Gomathi Sankareswari et al., 2014). For manganese(III) salophen there is a contradiction where Doctrow et al. (2002) found that it is able to protect the cells thru hydrogen peroxide scavenging; while Ansari et al. (2009) reported that it is able to kill breast cancer cells. ZnS is known to be less potent than the metal salophen mentioned earlier as ZnS could not carry out redox reaction (Brissos et al., 2013; Rani et al., 2021); however it is unknown how the toxicity of ZnS will be affected upon conjugating with GNP.

2.4.2 Toxicity of GNP

The toxicity of GNP shall be taken into consideration while synthesizing metal complexes gold nanoparticle conjugates. However, the inconsistency in experiment set up for research of GNP's toxicity has led to conflicting data as the toxicity of GNP depend on various factors like shape, surface charge, species of stabiliser, and size (N. Khlebtsov et al., 2011).

Goodman et al. (2004) shows that cationic GNP are more cytotoxic than anionic GNP. This is in line with E. E. Connor et al.'s (2005) study which shows that GNP with anionic charge (coated with biotin or citrate) are non-cytotoxic; GNP with cationic charge (coated

with CTAB) are cytotoxic. Niidome et al. (2006) also support the finding by discovering anionic GNP (coated with anionic PEG) is less cytotoxic. In the other hand, there is some disagreement from the findings obtained from Y. Zhang et al. (2012) and Schaeublin et al. (2011). Both of their studies state that there is no difference in the cytotoxicity of cationic and anionic GNP.

Besides, GNP are expected to show size depending toxicity as size is used to measure the uptake efficiency of GNP thru endocytosis (N. Khlebtsov et al., 2011). Pan et al. (2007) and Tsoli et al. (2005) reported that GNP with the diameter of 1-2 nm are highly cytotoxic; while 15 nm GNP are non-cytotoxic (Pan et al., 2007). Yah (2013) suggested that the toxicity of GNP increase when the size of GNP getting smaller.

Various studies also indicate that GNP with diameter ranging from 10 to 20 nm are non-cytotoxic (E. E. Connor et al., 2005; J. A. Khan et al., 2007; Murawala et al., 2009; Salmaso et al., 2009; Villiers et al., 2010); however, Pernodet et al. (2006) observed cell death in 15 nm GNP. Kim et al. (2008) found that GNP with size 20-100 nm are non-cytotoxic; while Mironava et al. (2010) found 45 nm GNP are more cytotoxic than GNP of 13 nm. Given the complexity of various physiochemical properties, this rises the need to examine the cytotoxicity of the new ZnS conjugated gold nanosphere.

2.5 Protein Interaction

Upon entering the blood circulation, drugs bind on plasma proteins to different extent where some binding is reversible and some binding establish an equilibrium (Vuignier et al., 2010). Among the proteins present in our plasma such as α1-acid glycoprotein, globulins and lipoproteins, serum albumin is the protein that present in the highest abundancy. The interaction between protein and drug will determine the fate of the drug as it will determine the availability of free drug. The availability in turn affects the pharmacodynamics and pharmacokinetics of the drug (Vuignier et al., 2010). The ability

to bind with albumin would improve the drug's solubility in plasma which in return increases the drug's plasma half-life and prevent them from encountering metabolic degradation (Ebrahimipour et al., 2017). Meanwhile, Ebrahimipour et al. (2017) also discovered that human serum albumin (HSA) tends to accumulate in cancer cells which could make protein act as an agent to deliver anticancer drugs.

Since bovine serum albumin (BSA) has high similarity with HSA (Michnik et al., 2006) and cost lesser, BSA is commonly used in laboratories to replace HSA in protein binding studies. Due to its high solubility, BSA are used to transport metal ions, steroids, fatty acids, metabolites and drugs (Asadi et al., 2016). Docking studies found that salophen complexes of nickel(II), uranium(VI), aluminium(III), gallium(III), indium(III), vanadium(IV) and manganese(III) could bind with BSA with strong affinity. (Asadi et al., 2016; Ebrahimipour et al., 2017; Gomathi Sankareswari et al., 2014; Mutua et al., 2019; V. Oliveri et al., 2011; Rani et al., 2021). Hence, it might be interesting to find out how would AuNS-TA-ZnS conjugates bind and interact with proteins.

CHAPTER 3: RESEARCH METHODOLOGY

3.1 Chemicals and Materials

All chemicals and solvents used were of analytical grade unless mentioned. Salicylaldehyde, 1,2-phenylenediamine, gold(III) chloride trihydrate, trisodium citrate dihydrate and thioctic acid were purchased from Sigma Aldrich. zinc(II) nitrate, absolute ethanol, methanol, acetic acid, hydrochloric acid, nitric acid, DMSO and chloroform were acquired from Fisher Scientific.

For protein interaction studies, Elisa grade BSA was obtained from Biochem and 20S mouse proteasome was acquired from Boston Biochem,

MCF-7 cell line (human breast cancer), MDA-MB-231 cell line (human breast cancer), MDA-MB-468 cell line (human breast cancer), and Caco-2 cell line (human colon cancer) were the cell lines used in the biological studies. All these cell lines were purchased from American Type Culture Collection (ATCC). Dulbecco's modified Eagle Medium (DMEM), fetal bovine serum (FBS), trypsin-EDTA, Tris-HCl and Hanks' buffer salt solution (HBSS) were purchased from Gibco. Trypan blue and 2′,7′-dichlorofluorescin diacetate (DCFH-DA) were obtained from Sigma Aldrich; phosphate buffer solution (PBS) and 4,5-dimethylthiazol-2-yl-2,5-diphenyltetrazolium bromide (MTT) were purchased from BioBasic.

3.2 Synthesis

3.2.1 Synthesis of Salophen

The Schiff base ligand, salophen (Figure 3.1) was synthesised by modification of the condensation method described by (Ouari et al., 2015). Herein, 10 mmol of salicylaldehyde and 5 mmol of 1,2-phenylenediamine were dissolved in 10 mL of absolute ethanol. The solution was continuously stirred and heated for 3 hours in the

presence of 2 – 3 drops of acetic acid. The yellow microcrystals of salophen were collected, filtered and washed three times with absolute ethanol.

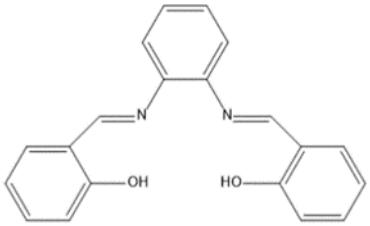

Figure 3.1: Chemical structure of salophen.

3.2.2 Synthesis of Zinc(II) Salophen (ZnS)

0.5 mmol of zinc(II) nitrate was dissolved in water and 0.5 mmol of salophen was dissolved in 10 mL of methanol separately. A yellow precipitate (Figure 3.2) was formed after the two solutions were mixed together and heated for 2.5 hours. The precipitate of ZnS was collected, filtered and washed three times with methanol.

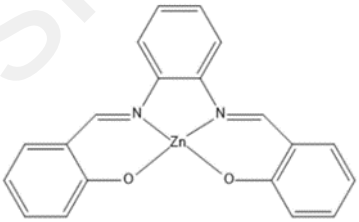

Figure 3.2: Chemical structure of zinc(II) salophen.

3.2.3 Synthesis of Gold Nanosphere (AuNS)

A modification of the Turkevich method (Turkevich et al., 1951) was used to synthesise AuNS. All glass wares were cleaned with aqua regia before synthesise. 2.5 mL of 0.01M of gold(III) chloride trihydrate was added to 50 mL of ultrapure water and heated to boil. Upon boiling, 4 mL of 0.03 M of trisodium citrate dihydrate was added and the heating was continued for another 15 minutes.

Upon the addition of trisodium citrate dihydrate, the pale-yellow colour of gold(III) chloride solution changed from grey to purple and became wine red colour. The AuNS solution was cooled down to room temperature and ultracentrifuged (Beckmann Conter) at 11000 rpm for 20 minutes. The supernatant was removed and the AuNS pellet was recovered.

3.2.4 Functionalisation of Gold Nanosphere with Thioctic Acid (AuNS-TA)

The AuNS pellet was diluted with 10 mL of pH 14 ultrapure water which was pre-adjusted with 1M sodium hydroxide solution. A 1 mL of 0.05 M thioctic acid was dissolved in absolute ethanol before being added to the AuNS solution. After stirring for 24 hours in dark, the mixture was ultracentrifuged at 11000 rpm for 20 minutes. The supernatant was then removed and the AuNS-TA pellet was recovered.

3.2.5 Conjugation of ZnS with AuNS-TA (AuNS-TA- ZnS)

The AuNS-TA pellet was diluted with 10 mL of pH 14 ultrapure water. 1 mL of 1 nM ZnS was dissolved in 1:1 DMSO: ethanol and added to the AuNS-TA solution. The mixture was stirred in the dark at room temperature for 24 hours before being ultracentrifuged at 10 000 rpm for 20 minutes. The supernatant was removed to recover the pellet of AuNS-TA-ZnS and followed by washing with chloroform for three times.

3.3 Characterisation

3.3.1 Fourier Transform Infrared (FTIR) Spectroscopic Analysis

Prior to analysis, the solutions of AuNS, AuNS-TA, and AuNS-TA-ZnS were freeze under -80 ℃ for 24 hour and was later subjected to freeze drying with freeze dryer at -80 mbar for 24 hours to obtain their respective powders The powdered samples were analysed with attenuated total reflectance (ATR) and the infrared transmission spectra of all samples were recorded from 400 cm^{-1} to 4000 cm^{-1} using Shimadzu Fourier Transform Infrared Spectroscopy IRTracer-100.

3.3.2 CHN Elemental Analysis

Around 5 mg of sample was weight and wrapped in tin capsule manufactured by Perkin Elmer. After the decomposition of sample in the combustion chamber, the composition of Carbon, Hydrogen and Nitrogen was measured by Perkin Elmer Series II CHNS/O Analyzer.

3.3.3 Ultraviolet-Visible (UV-Vis) Spectroscopic Analysis

Salophen and ZnS were dissolved in a solvent mixture of DMSO: ethanol in a 1:1 ratio; while AuNS, AuNS-TA, and AuNS-TA-ZnS pellet were redispersed in pH 14 ultrapure water. The solution was filled into a Quartz cuvette with 1 cm path length and the spectrum was recorded from 200 cm^{-1} to 1000 cm^{-1} with Perkin Elmer UV/VIS Spectrometer Lamda 25.

3.3.4 Fluorescence Spectroscopic Analysis

Salophen and ZnS were dissolved in a solvent mixture of DMSO: ethanol in a 1:1 ratio; while AuNS, AuNS-TA, and AuNS-TA-ZnS pellet were redispersed in pH 14 ultrapure water. The solution was filled into a Quartz cuvette and excited at different wavelength. The fluorescent emission spectrum was then recorded by Cary Eclipse Fluorescence Spectrophotometer from Agilent Technologies.

3.3.5 Dynamic Light Scattering and Zeta Potential Analysis

The size and Zeta potential of AuNS, AuNS-TA, and AuNS-TA-ZnS were measured at 25 ℃ with Malvern Zetasizer nano ZS particle size analyser with DTS1070 cuvette. During the analysis of nanoparticles size, DLS was detected at an angle of 173˚. Each analysis was carried out thrice with each measurement of 25 runs.

3.3.6 Transmission Electron Microscopy (TEM)

AuNS, AuNS-TA, and AuNS-TA-ZnS nanoparticles were placed on graphene coated Copper TEM grids by immersing the grids into the nanoparticles sample solutions. After the grids has been air dried, it was then inserted into the Tecnai G2 20 TEM and images of the nanoparticles were captured at 200 kV.

The diameter of 100 nanoparticles were measured with Image J to obtain the average size and standard deviation of AuNS, AuNS-TA, and AuNS-TA-ZnS nanoparticles

3.3.7 Inductively Coupled Plasma Mass Spectroscopic (ICP-MS) Analysis

AuNS-TA-ZnS pellet was redispersed in pH 14 water. 15 mL of 1 nM AuNS-TA-ZnS was prepared in a 50 mL centrifuge tube. The amount of zinc atoms and gold atoms present in the solution was determined by using Perkin Elmer Elan 9000 ICP/MS. The loading capacity of ZnS on AuNS-TA-ZnS was then calculated as described in section 4.1.7.

3.4 Protein Interaction Studies

3.4.1 Bovine Serum Albumin (BSA) Interaction Study *via* Fluorescence Spectroscopy

A 10 μM of BSA was prepared in phosphate buffer solution (PBS) (pH 7.4) at room temperature. BSA was mixed with different volumes of 1 nM AuNS-TA-ZnS nanoparticles solution to obtain a series of AuNS-TA-ZnS solutuions with their concentrations ranging from 15.625 pM to 250 pM and a final volume of 4 mL. After 2 hours of incubation, the fluorescence spectra of the above series were recorded at λ_{ex} = 280 nm and λ_{em} = 300 to 450 nm.

The fluorescence emission spectra of the AuNS-TA-ZnS series (at concentration ranging from 15.625 pM to 250 pM) without the presence of BSA were also obtained and subtracted with their corresponding spectrum of BSA and AuNS-TA-ZnS mixtures.

Synchronous florescence scanning was carried out on mixture of BSA and AuNS-TA-ZnS at $\Delta\lambda$ = 15 nm and 60 nm for tyrosine and tryptophan residues respectively.

3.4.2 BSA Interaction Study *via* Circular Dichroism (CD)

A solution of 10 µM BSA was prepared in PBS; while a stock solution of 50 pM AuNS-TA-ZnS was prepared at pH 14. 100 µL of 10 µM BSA was mixed with 100, 200, 300, 400, 500 µl of stock AuNS-TA-ZnS solution. The resultant series of solutions were topped up to 1 mL with PBS to yield AuNS-TA-ZnS at final concentrations ranging from 0.005 – 0.025 pM (0.005, 0.010, 0.015, 0.020, 0.025 pM).

After 30 minutes of incubation, the CD spectra of the series of BSA and AuNS-TA-ZnS mixture were recorded with Jasco J-815 CD spectrometer. The samples were read with a 1 cm cuvette at 0.2 nm intervals. Scans were performed from 185 - 300 nm and shown as ellipticity in millidegree.

3.4.3 20S Mouse Proteasome Activity Study

Trypsin-like (T-L), chymotrypsin-like (CT-L) and caspase-like (C-L) proteolytic activities on 20S proteasome can be measured by using their respective fluorogenic peptide substrates which are Boc-Leu-Arg-Arg-AMC, Suc-Leu-Leu-Val-Tyr-AMC and Z-Leu-Leu-Glu-AMC (Suc: N-Succinyl; Z: benzyloxycarbonyl; Boc: t-Butyloxycarbonyl; AMC: 7-amino-4-methylcoumarin).

A solution of 14 µL of activated purified 20S mouse proteasome (2 nM per well), 20 µL of 20 µM of fluorogenic peptide substrate (4 µM per well) and appropriate volume of AuNS-TA-ZnS at indicated concentration (2.5, 5.0, 10, 20, 30, 40, 60 x 10¬-6 nM) were

added into each well of the 96-well plate. The final volume of each well was made to be 100 uL by the addition of 50 mM Tris HCl (pH 7.5). Control wells were also prepared with the materials mentioned above in the absence of AuNS-TA-ZnS.

After 24 hours of incubation at 37 °C, SpectraMax M5 was used to measure the fluorescence intensity of the cleaved fluorogenic groups at an excitation wavelength of 380 nm and emission wavelength of 460 nm. Proteolytic activity of each well was calculated with the following equation and the proteolytic activity for each site at different concentrations of AuNS-TA-ZnS was plotted on a graph.

$$\text{Proteolytic activity (\%)} = \frac{\text{Fluorenscence intensity of sample}}{\text{Fluorescence intensity of control}}\ x\ 100 \qquad (3.1)$$

3.5 Biological studies

All the cell lines were cultured in T-25 or T-75 flask and maintained in an incubator with 5% carbon dioxide. When the confluency reached 80 to 90%, cells were detached from the flask with trypsin-EDTA and harvested into a 15 mL centrifuge tube for a 5 minutes centrifugation at 1500 rpm. The cell pellet was collected and redistributed in the media. The cell number in the cell suspension solution was determined using hemacytometer with trypan blue staining the live cells.

3.5.1 Cell Viability Assay

Cells were seeded at the density of 1 x 10^4 cells/well in transparent 96-well plate. After an incubation of 24 hours in 5 % of carbon dioxide, the media in the wells were removed and treated with sample solutions at concentrations ranging from 0 – 1 nM. The cells were then incubated for another 48 hours. Upon the endpoint, 20 uL of 5 mg/mL MTT solution was inserted to each well and was incubated for another 4 hours to form formazan crystals. The mixture of solutions in each well was then removed and replaced with 80 μL of DMSO to dissolve the formazan crystals.

The ultraviolet absorbance of each well at 570 nm was then measured with Spectramax M3 with 630 nm as the reference wavelength. The cell viability of each well was calculated by using the following formula.

$$\text{Cell viability (\%)} = \frac{\text{Sample Absorbance}}{\text{Control Absorbance}} \text{ x } 100\% \quad (3.2)$$

3.5.2 Intracellular Reactive Oxygen Species (ROS) Assay

Cells were seeded at the density of 1 x 10^4 cells/well in black 96-well plate and incubated for 24 hours under 5 % of carbon dioxide. The media in the well was removed on the next day and replaced with sample solutions at different concentrations. After 24 hours, the solution mixture was removed from the well, and each well was washed with 80 µL of PBS. 100 µL of fresh media which contains 20 µM of 2′,7′-dichlorofluorescin diacetate (DCFH-DA) was added to each well.

When excited at 485 nm, the intensity of the fluorescent emitted at 535 nm for each well was measured by TECAN microplate reader and the readings were labelled as T_0. The cells were incubated for another 30 minutes, and the previous steps were repeated again with the readings labelled as T_f. The ROS level of each well was calculated with the following equation.

$$\text{ROS level} = \frac{\text{Fluorescence intensity at } T_f - \text{Fluorescence intensity at } T_0}{\text{Cell viability percentage}} \quad (3.4)$$

Upon obtaining the ROS level of each well, fold change of ROS can be calculated by using the following equation.

$$\text{Fold change of ROS} = \frac{\text{ROS level of well with treated cell}}{\text{ROS level of well with untreated cell}} \quad (3.5)$$

3.5.3 TEER Measurement Assay

Caco-2 cells were seeded at 1 x 10^6 cells/well on each Corning transwell insert made of polycarbonate membrane with a growth area of 0.33 cm^2 and pore size of 0.4 μm. Cells were cultured continuously for 21 days where the media in each well was changed every 2 days. The integrity of the cell monolayer was evaluated by measuring the TEER with EVOM2 Epithelial Volt/Ohm Meter.

After 21 days, the cells were washed with HBSS and replenished with fresh media. AuNS-TA-ZnS and ZnS of different concentrations were added to the apical chamber of the transwell insert and the cells were incubated again. TEER readings of each well were taken every 30 minutes for 8 times and plotted on a graph.

CHAPTER 4: RESULTS AND DISCUSSIONS

4.1 Characterisation

4.1.1 Fourier Transform Infrared (FTIR) Spectroscopy

The spectrum of salophen (Figure 4.2) shows a band at 3055 cm^{-1} indicates the presence of phenolic OH group. A strong band presents at 1608 cm^{-1} is ascribed to the combination of C=N stretching and C=C aromatic vibration stretching (Mota et al., 2012). Other bands of C=C aromatic vibration stretching are found at 1558 cm^{-1} and 1190 cm^{-1} (Mota et al., 2012). The strong band which emerges at 1275 cm^{-1} could be assigned to phenolic C-O stretching (Dong et al., 2012; Mota et al., 2012); while the other band at 754 cm^{-1} is reported to be an aromatic C-H stretching (R. A. Mendes et al., 2018).

From the ZnS spectrum (Figure 4.3), the combination of C=N stretching and C=C aromatic vibration stretching band has shifted to a higher frequency, 1612 cm^{-1} upon the formation of ZnS. Bands of C=C aromatic stretching shift to a lower frequency (1529 cm^{-1} and 1174 cm^{-1}) (Tverdova et al., 2009) and the same goes to the phenolic C-O stretching band which undergoes a redshift to 1244 cm^{-1}. Hence, Dong et al. (2012) and More et al. (2017) suggest that Zn-O bond has been established between zinc(II) ion and the free ligand. The aromatic C-H bending of the free ligand which is initially at 754 cm^{-1} shifted to 746 cm^{-1} after the formation of ZnS. A metal-oxygen (M-O) stretching band (More et al., 2017) at 532 cm^{-1} further suggests the coordination of salophen to zinc(II) ion.

As the surface of AuNS is covered with a layer of citrate ions, the OH group of citrate acid gave rise to a broad O-H stretch in the spectrum of AuNS (Figure 4.4) at 3298 cm^{-1}. Bands at 1614 cm^{-1} and 1348 cm^{-1} are assigned to the asymmetric and symmetric stretching of the free carboxylate group (O=C=O) (Aryal et al., 2006; Kalimuthu et al., 2010). These bands are absent in the spectrum of AuNS-TA (Figure 4.5) upon the replacement of citrate acid by thioctic acid.

From AuNS-TA spectrum (Figure 4.5), the broad peak at 3233 cm^{-1} is due to the O-H stretch of thioctic acid. The spectrum also exhibits a C-H stretching band at 2922 cm^{-1} (Young et al., 2007); while peaks at 1743 cm^{-1} and 1649 cm^{-1} are symmetric and asymmetric C=O stretching (Ikuta et al., 2014; Kataby et al., 1999). O-H stretching band can be found at 1045 cm^{-1}. According to Rosenthal-Kim (2013), the bands at 663 cm^{-1} and 457 cm^{-1} are a result of C-S stretch and S-S stretch of thioctic acid respectively.

The absence of the broad O-H band at the 3000-3300 cm^{-1} region of AuNS-TA-ZnS spectrum (Figure 4.6) suggests the deprotonation of the carboxylic group of thioctic acid in AuNS-TA and the coordination of the carboxylate oxygen with ZnS. Peaks located within 1600 – 1700 cm^{-1} might be the bands of C=O stretch from thioctic acid and C=N & C=C stretch of ZnS. The sharp peaks around 822 cm^{-1} could be assigned to C-H stretch of both thioctic acid and ZnS that shifted to a higher frequency upon conjugation of AuNS-TA with ZnS. The blueshift also happened to C-S stretching band which moved to 710 cm^{-1} after coordination.

Thus, with the aid of TA as linker, AuNS-TA-ZnS was synthesised. The corboxylate end of TA conjugated with ZnS; while the thiol ends of TA anchored on AuNS via the strong gold-thiol covalent bond (Yeh et al., 2021) as illustrated in Figure 4.1.

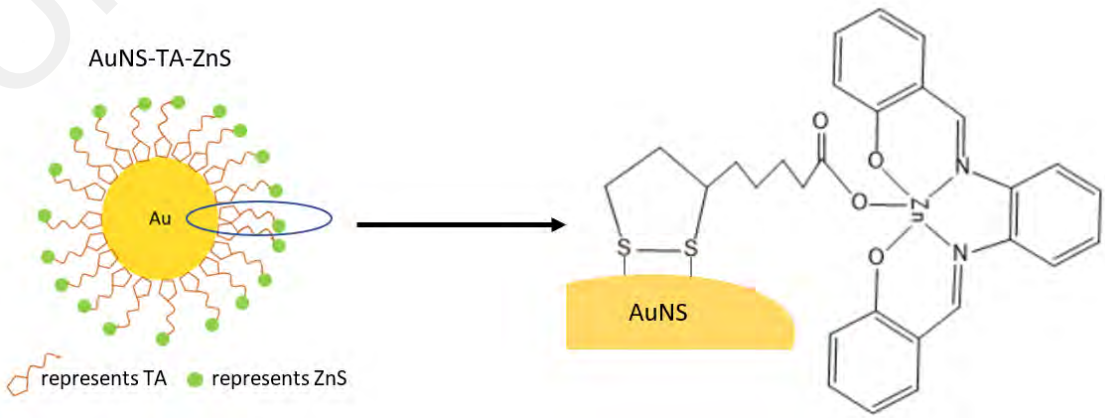

Figure 4.1: Illustration of AuNS-TA-ZnS structure

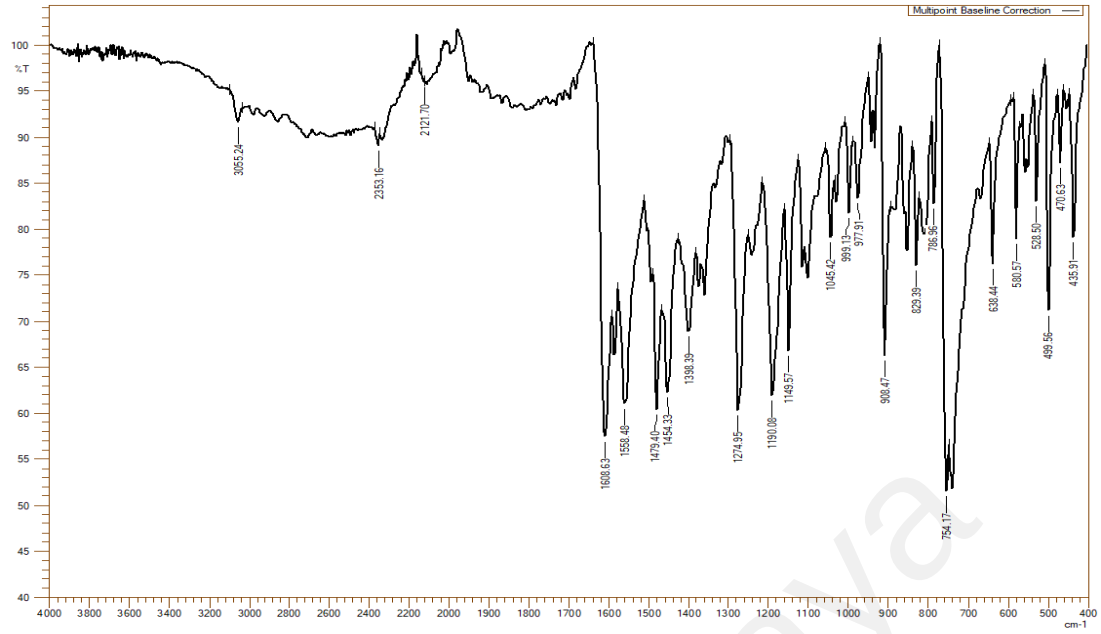

Figure 4.2: FTIR spectrum of salophen.

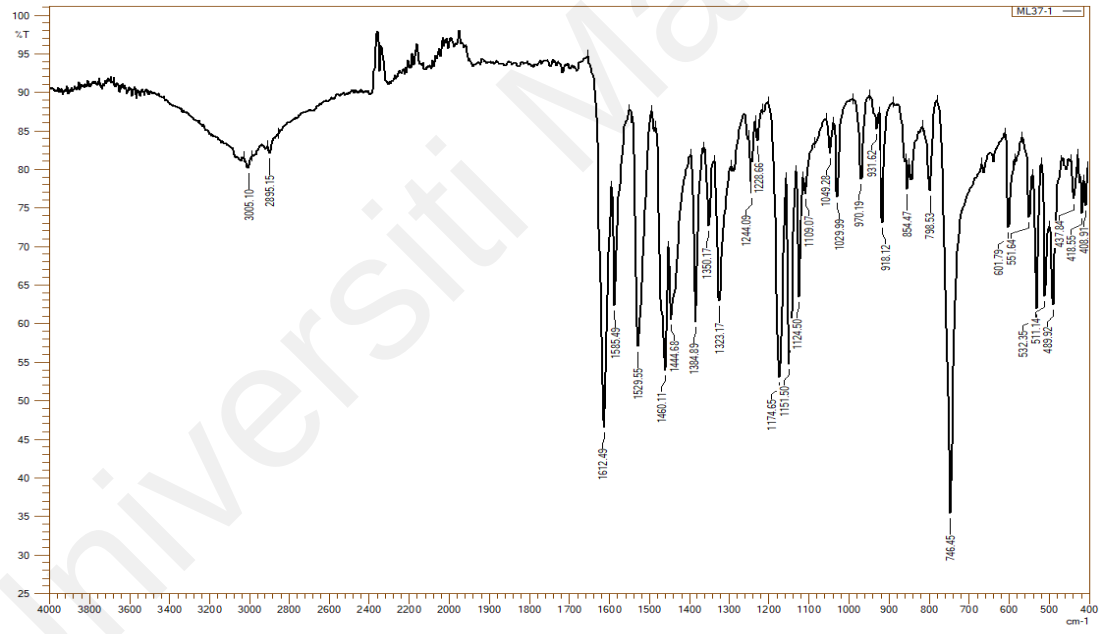

Figure 4.3: FTIR spectrum of ZnS.

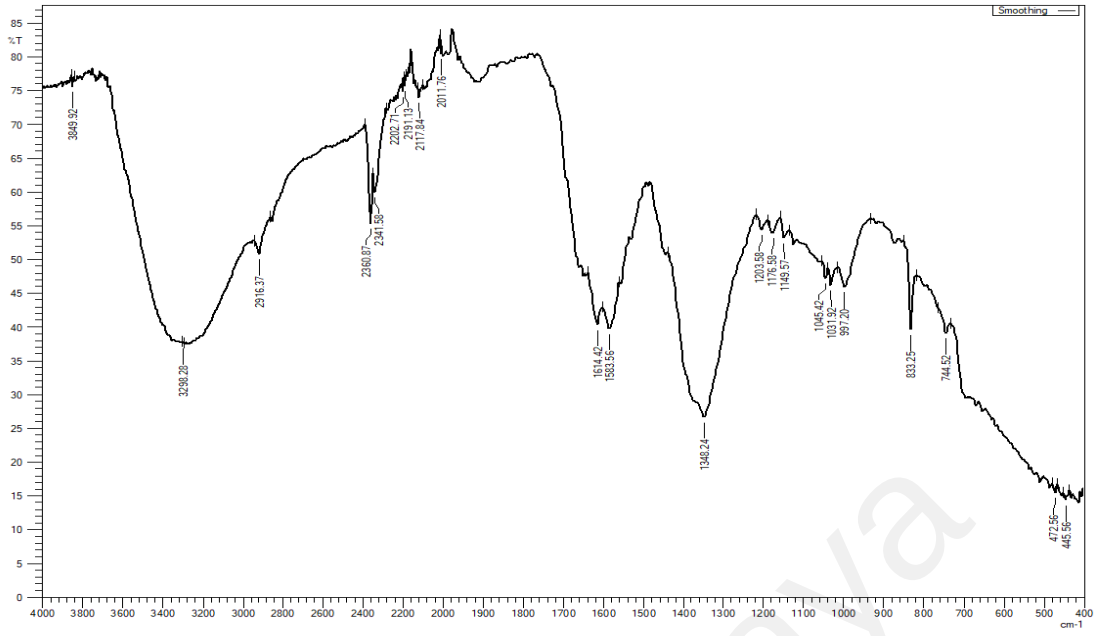

Figure 4.4: FTIR spectrum of AuNS.

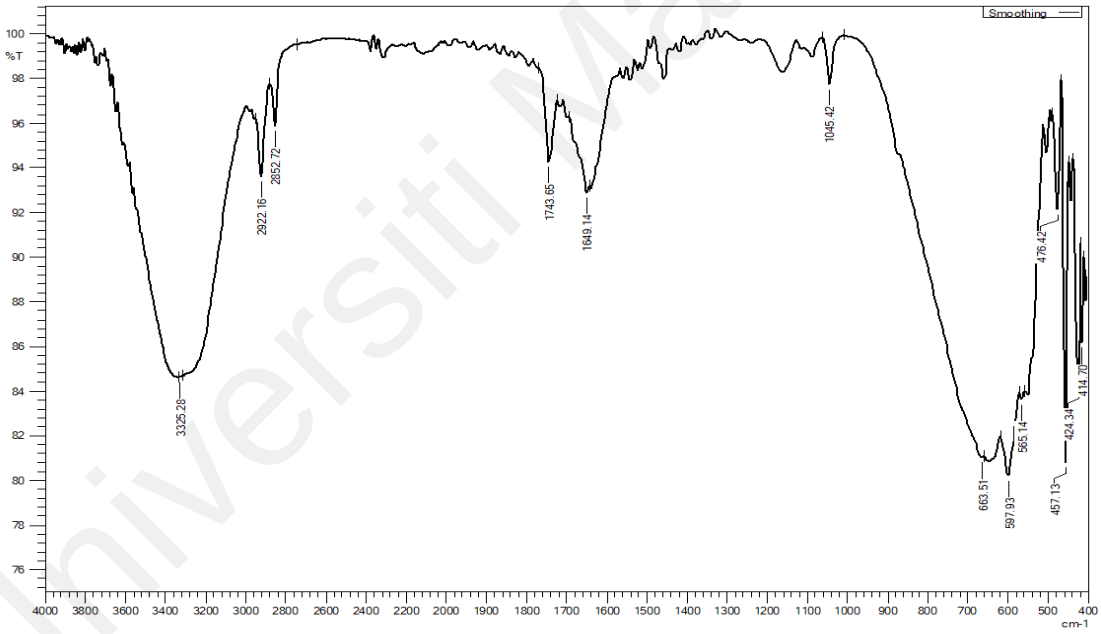

Figure 4.5: FTR spectrum of AuNS-TA.

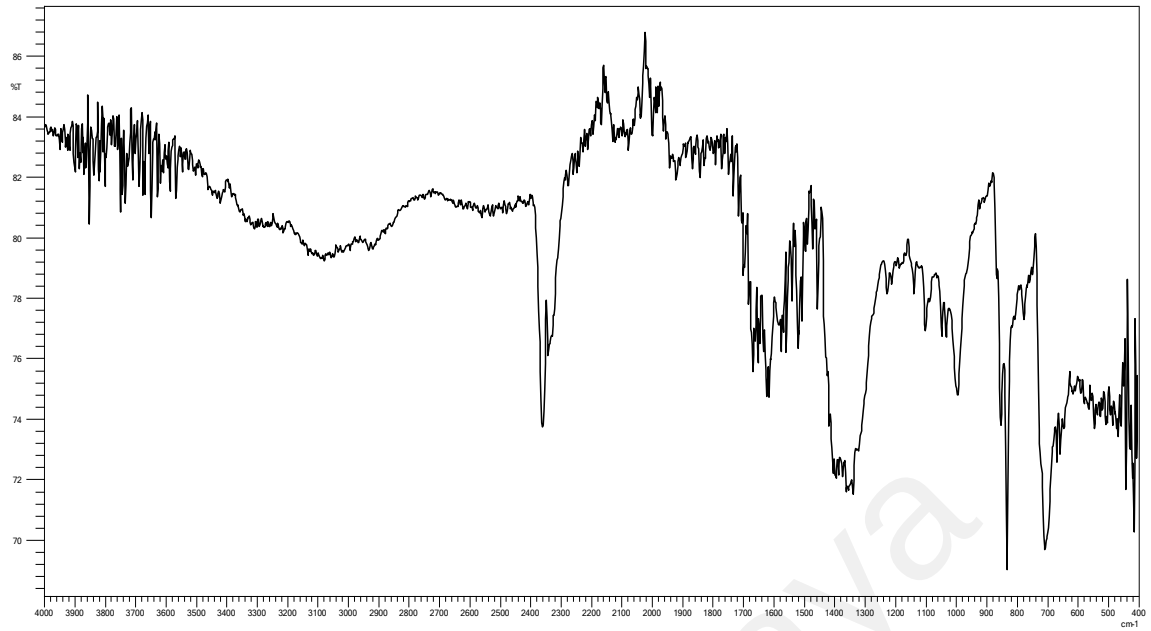

Figure 4.6: FTIR spectrum of AuNS-TA-ZnS.

4.1.2 CHN Elemental analysis

Table 4.1: Stoichiometries, colour and elemental analysis of salophen and zinc(II) salophen.

Compound	Stoichiometries	Colour	Analysis Calculation (Found) %		
			C	H	N
Salophen	$C_{20}H_{16}N_2O_2$	Yellow	75.93 (75.55)	5.10 (5.21)	8.86 (8.98)
Zinc(II) Salophen	$[Zn(C_{20}H_{16}N_2O_2)].2H_2O$	Yellow	57.77 (57.77)	4.36 (4.99)	6.74 (7.56)

The CHN elemental analysis results are in good agreement with the postulated chemical formulae. The difference in %C, %H and %N values between postulated and found values were within 1%, and the postulated formulae are therefore acceptable. The chemical formula of Salophen is determined to be $C_{20}H_{16}N_2O_2$ (molecular weight: 316.36

g mol^{-1}); while the chemical formula for ZnS is $[Zn(C_{20}H_{16}N_2O_2)].2H_2O$ (formula weight: 417.77 g mol^{-1}).

4.1.3 UV-Vis Spectroscopic Analysis

Both salophen and ZnS consist benzene rings and imine groups. In the UV-vis spectrum of salophen (Figure 4.7), the benzene rings exhibit a π -> π* electronic transition at 274 nm (Ouari et al., 2015); while the absorption band at 333 nm could be assigned to the n -> π* electronic transition of the non-bonding electron from imine groups (Gusev et al., 2020). Both bands experienced a blue-shift to 260 nm and 295 nm after coordinating with zinc(II) ion which resembles the observation from El-Medani et al. (2005) amd Shaghaghi et al. (2020).

The peak at 395 nm (Figure 4.7) which only emerged after the formation of ZnS may be assigned as metal-ligand d-> π* charge transfer (MLCT) transition (Dumur et al., 2014). Since zinc(II) ion has a d10 electronic configuration, thus d-d transition would not be observed (Shaghaghi et al., 2020).

Table 4.2: Electronic spectral assignment.

Compound	Electronic spectrum (nm)	Electronic Transition	Molar absorptivity, ϵ (M^{-1} cm^{-1})
Salophen	274	π -> π*	2.8×10^3
	333	n -> π*	1.6×10^3
Zinc(II) Salophen	260	π -> π*	5.6×10^3
	295	n -> π*	1.4×10^4
	393	MLCT	1.2×10^4

The spectra of AuNS, AuNS-TA and AuNS-TA-ZnS nanoparticles (Figure 4.7) exhibit an absorption peak around 521 nm due to the SPR effect (Haiss et al., 2007). Plasmon can be understood as the coherent oscillation of free d electrons in the gold metal (Eustis

et al., 2006) from its equilibrium position (Navarrete et al., 2018). When the wavelength of the light received by the nanoparticles is in resonance with the frequency of oscillation, the electron cloud will polarise to one end of the surface and oscillation starts (Amendola et al., 2017).

The SPR peak of AuNS-TA-ZnS experienced a red shift to 523 nm when compared to AuNS. The decrease in the resonance frequency is a result of the alteration on the surface electron density which could be due to the present of chemically bonded molecules (Eustis et al., 2006). This may suggest that the conjugates of AuNS-TA-ZnS have been synthesised. Besides, the presence of a small and broad peak at 403 nm might be related to the red shift of MLCT band of ZnS upon conjugation of ZnS with AuNS-TA.

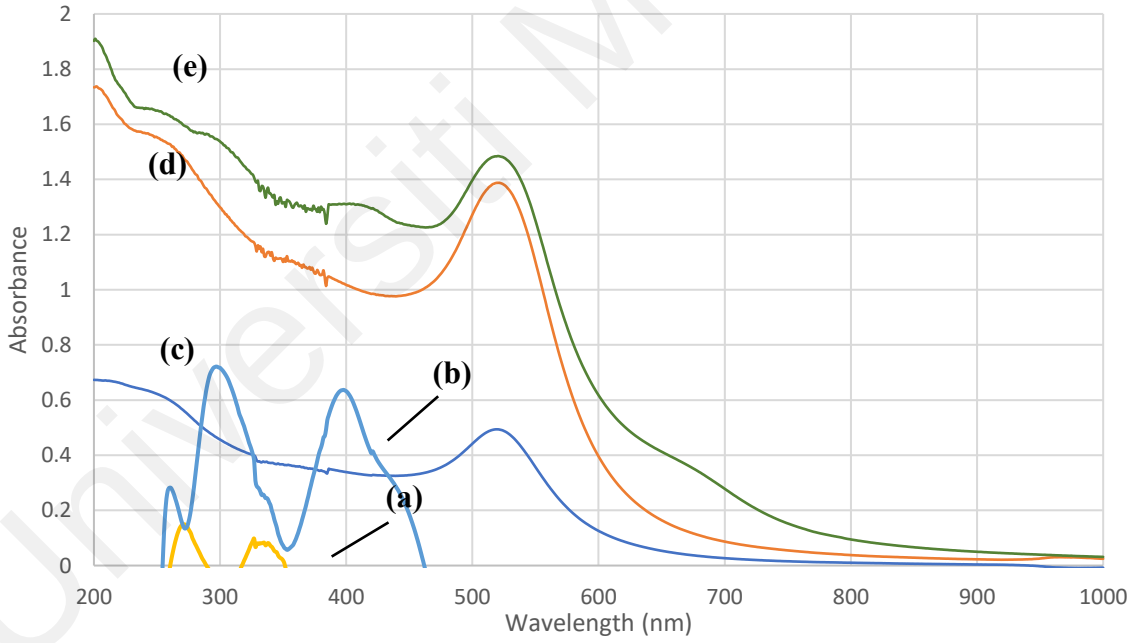

Figure 4.7: UV-visible spectrum of (a) salophen (b) ZnS (c) AuNS (d) AuNS-TA (e) AuNS-TA-ZnS

4.1.4 Fluorescence spectroscopy

From figure 4.8, it was observed that ZnS excites at 393 nm and emits fluorescent at 503 nm. The fluorescence of ZnS was greatly enhanced after salophen coordinated with zinc(II) ion to form ZnS. T. Khan et al. (2016) with a similar finding explained that this

is due to ZnS is unable to carry out imine-enamine tautomerization like salophen. Thus, ZnS becomes more rigid after the coordination which results to an increase in quantum yield and fluorescence enhancement.

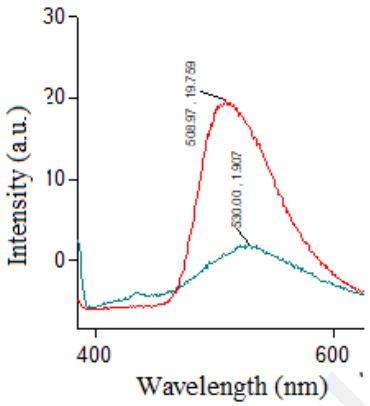

Figure 4.8: Emission spectra of 50 uM of ZnS (red) and 50 uM of salophen (green) excited at 393 nm.

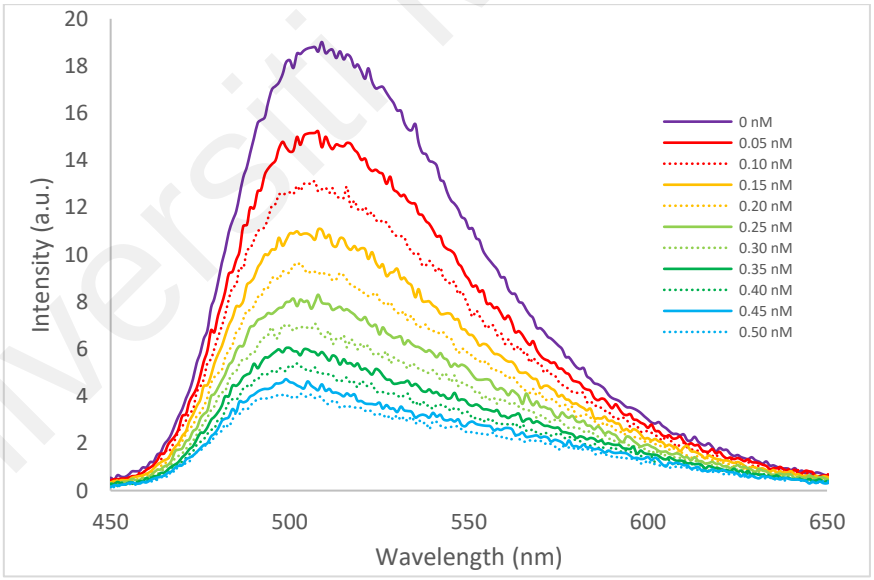

Figure 4.9: Emission spectra of 50 uM ZnS (excited at 393 nm) in the presence of AuNS-TA in various concentration.

On the other hand, AuNS, AuNS-TA and AuNS-TA-ZnS do not emit fluorescence. It was believed that enhancement in fluorescence emission can be achieved by conjugating a fluorophore which has an emission wavelength overlapped with the adsorption wavelength of metal nanoparticle. As this would allow an efficient excitation and energy

transfer, staging a better metal enhanced fluorescence (MEF) to occur (Han et al., 2011; Kondon et al., 2008; Pompa et al., 2006).

Unfortunately, in this study, the above phenomenon does not occur although ZnS (the fluorophore) emits at 503 nm; while AuNS-TA features an excitation peak at 520 nm. As shown in figure 4.9, the fluorescence of ZnS decreases when more AuNS-TA nanoparticles were added to form AuNS-TA-ZnS.

Various studies (Chen et al., 2007; Dulkeith et al., 2005; Reineck et al., 2013) explained that the enhancement or quenching of fluorescence depends on the distance of fluorophore to the metal nanoparticle. When the distance is below 5 nm (Anger et al., 2006), non-radiative decay occurs. This causes the energy of the fluorophore being channelled from the excited dipole to the nanoparticles where plasmon are excited, leading to quenching in emission (Kochuveedu et al., 2014; Yuan et al., 2020). This resembles the finding obtained in this study as AuNS and ZnS are connected by thioctic acid which its distance is less than 5 nm.

4.1.5 DLS and Zeta Potential Analysis

DLS technique was employed in this experiment to give an estimation on the diameter of the GNP. Table 4.3 shows that the average diameter of AuNS is measured to be 20.94 nm, which become slightly larger, 21.94 nm after surface functionalisation with thioctic acid.

Although the surface charge of nanoparticles could not be measured directly via zeta potential; however, it is seen as a function of surface charge (Bruce B. Weiner, 1993). AuNS and AuNS-TA exhibit a negative potential of -45.87 mV and -54.9 mV due to their surfaces are capped with citrate and thioctate groups which bear negative charges. Zeta potential with a magnitude greater than +/- 30 mV symbolises that the nanoparticles have

sufficient repulsive force to ensure its' physical stability (Bhattacharjee, 2016; Joseph et al., 2019).

For AuNS-TA-ZnS, since some of the thioctate groups on the surface of AuNS-TA have conjugated with ZnS, the zeta potential decreases to -28.5 mV which indicates that the repulsive forces between nanoparticles decreased. As a result, aggregation could happen and nanoparticles form clusters. From Table 4.3, we could observe the polydispersity index of AuNS and AuNS-TA which range between 0.15 - 0.21 increases to 0.54 for AuNS-TA-ZnS, indicates that AuNS-TA-ZnS has a higher particle size population than AuNS and AuNS-TA (Danaei et al., 2018).

The AuNS-TA-ZnS nanoparticles which aggregated to form clusters will scatter more light (Bhattacharjee, 2016; Sergeev et al., 2013), causing DLS analysis to assign AuNS-TA-ZnS a larger diameter, 58.66 nm. Bhattacharjee (2016) and B. N. Khlebtsov et al. (2011) also reported that the particle size obtained from DLS analysis often appear to be larger than TEM analysis.

Table 4.3: DLS and zeta potential analysis of GNP

	Diameter (nm)	Polydispersity Index	Zeta Potential (mV)
AuNS	19.55	0.15	-46.4
	21.45	0.20	-48.1
	21.83	0.21	-43.1
Average	20.94 $\pm$ 1.22	0.19	-45.87 $\pm$ 2.54
AuNS-TA	21.34	0.19	-55.0
	22.24	0.17	-54.4
	22.23	0.20	-55.3
Average	21.94 $\pm$ 0.52	0.18	-54.9 $\pm$ 0.5

Table 4.3, continued

	Diameter (nm)	Polydispersity Index	Zeta Potential (mV)
AuNS-TA-ZnS	59.79	0.53	-28.1
	59.34	0.53	-29.1
	56.85	0.57	-28.4
Average	58.66 ± 1.58	0.54	-28.5 ± 0.5

4.1.6 TEM Analysis

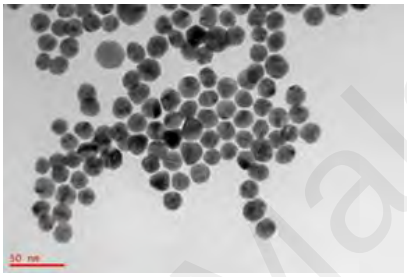

Figure 4.10: TEM image of AuNS.

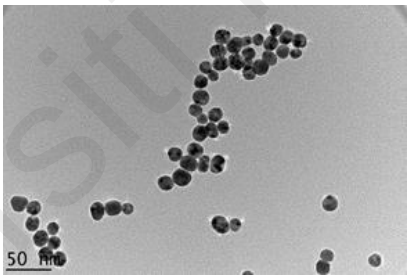

Figure 4.11: TEM image of AuNS-TA.

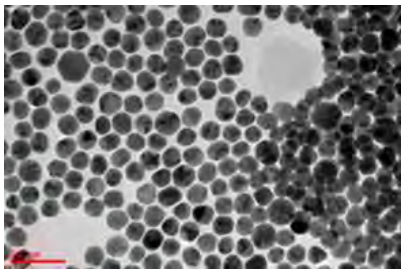

Figure 4.12: TEM image of AuNS-TA-ZnS.

From the TEM images, it is observed that most nanoparticles are spherical in shape. Nanoparticles of AuNS and AuNS-TA are separated from each other while AuNS-TA-ZnS nanoparticles exhibit sign of aggregation. The average diameter of AuNS is 14.97 ± 1.69 nm. It increases to 17.54 ± 1.60 nm after surface modification with thioctic acid to

form AuNS-TA and further increases to 17.73 ± 1.52 nm after conjugating with ZnS to form AuNS-TA-ZnS.

4.1.7 ICP-MS Analysis

Concentration of Au atom and Zn atoms found from ICP-MS analysis are 499.86 ug/L and 1.72 ug/L respectively. By assuming all the AuNS-TA-ZnS nanoparticles are spherical in shape and have a density resembling face-centred cubic GNP (Mucic et al., 1998), the following equation is used to calculate the average gold atoms in each nanoparticle, N:

$$N = \frac{N_A \pi_{,} p D^3}{6M} \tag{4.1}$$

where N_A is the Avogadro constant, ,p is the density for face-centred cubic GNP (1.93 x 10^{-20} g/nm^3) (H. Zhang et al., 2004), D is the diameter of nanoparticle and M is the atomic weight of gold.

In the above calculation, AuNS-TA-ZnS which has an average diameter of 17.73 nm have approximately 1.7 x 10^5 gold atoms per nanoparticle. By comparing the concentration of AuNS-TA-ZnS with the concentration of zinc atom found in the test sample, we may conclude that there are 1785 ZnS molecules conjugated to each single AuNS-TA nanoparticle.

4.2 Protein Interaction Studies

4.2.1 BSA Interaction Study via Fluorescence Spectroscopy

BSA protein molecule contains around 600 amino acids residue which were arranged into three helical domains. Among these domains, there are six binding sites with different binding affinity (Ng et al., 2013). In order to study the interaction between the binding of BSA and AuNS-TA-ZnS, residues that emit intrinsic fluorescence, such as tryptophan

(Trp), tyrosine (Tyr) and phenyalanine (Phe) become our main interest. However, the quantum yield of Phe is too low to be investigate; while Tyr which excites at the same wavelength as Trp often has its emission quenched in native protein (Ghisaidoobe et al., 2014). Thus, Trp becomes the dominant residue that excite at 280 nm and emit fluorescence at 350 nm.

There are two Trp residues in each BSA molecule, namely Trp134 and Trp213. The former is located in a hydrophobic pocket on the domain I's surface; while the latter is in a hydrophobic pocket in domain II (Carter et al., 1994). According to X. Shi et al. (2012), Trp residue has a relatively large excited state dipole moment which causes the fluorescence emission of Trp to be highly sensitive to the environment's polarity. Therefore, by monitoring the fluorescence emission of Trp, the protein conformational behavior around Trp residues could be predicted (Shang et al., 2007).

Figure 4.13 shows the fluorescence emission at 350 nm decreases gradually as concentration of AuNS-TA-ZnS increases. This indicates the presence of AuNS-TA-ZnS has quenched the fluorescence of Trp residues due to GNP behaving like an excited state quenchers through its energy transfer behaviour. No blue-shift or red-shift is being observed. Blue-shift will happen when BSA undergoes tertiary structural change to make the environment around the Trp residues become more hydrophobic; while red-shift happens when Trp residues are more exposed to the hydrophilic (solvent) environment (Shang et al., 2007). With that, we could assume that there is no conformational change happened upon binding of AuNS-TA-ZnS to BSA.

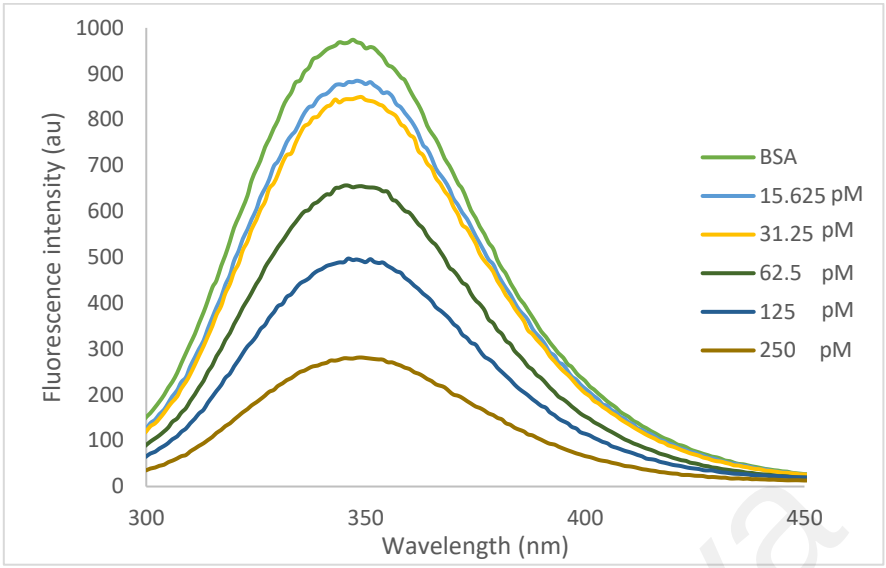

Figure 4.13: Fluorescence spectra of BSA + AuNS-TA-ZnS at concentration ranging from 0- 250 pM.

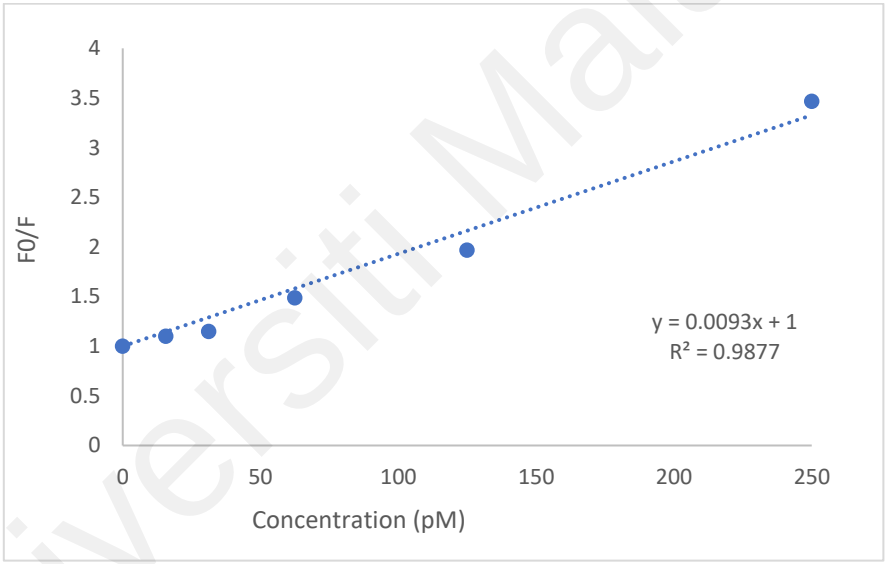

Figure 4.14: Stern-Volmer Plot.

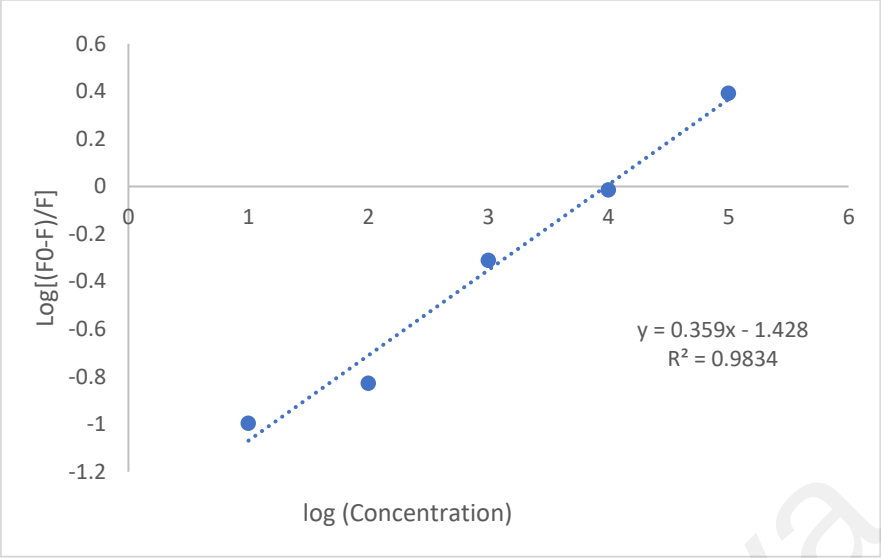

Figure 4.15: Scatchard Plot.

The fluorescence quenching was analysed with the Stern-Volmer equation (4.2) and Scatchard equation (4.3) (Sułkowska, 2002) to obtain more parameters.

$$\frac{F_0}{F} = 1 + k_q \tau_0 [Q] = 1 + K_{sv}[Q] \quad (4.2)$$

$$\log\left(\frac{F_0 - F}{F}\right) = \log K_b + n \log[Q] \quad (4.3)$$

Where F_0 is the relative fluorescence intensity in the absence of quencher, F is the relative fluorescence intensity in the presence of quencher, k_q is the bimolecular quenching rate constant, τ_0 is the average lifetime of BSA in the excited state 5 x 10^{-9} s, K_{sv} is the Stern-Volmer dynamic quenching constant, [Q] is the concentration of quencher, K_b is the binding constant of quencher with BSA and n is the number of binding sites. These parameters are obtained by plotting the Stern-Volmer plot and Scatchard plot as shown in figure 4.14 and figure 4.15.

The quenching rate constant, k_q obtained from the Stern-Volmer plot is 1.86 x 10^{18} mol^{-1} s^{-1} which is much greater compare to the maximum value for a diffusion-controlled quenching (~ 2 x 10^{10} mol^{-1} s^{-1}). This suggests that the quenching mechanism was initiated by a static quenching process instead of a dynamic quenching process (Suryawanshi et

al., 2016) where a ground state conjugate is formed between AuNS-TA-ZnS and BSA (Comby et al., 2011; Ghisaidoobe et al., 2014; Kang et al., 2004).

The calculated Stern-Volmer quenching constant, K_{sv} is 9.3 x 10^9 M^{-1}, implying that AuNS-TA-ZnS has a strong quenching ability (X. Shi et al., 2012). A material is called as a superquencher when its K_{sv} is at 10^4 M^{-1} or higher (Achyuthan et al., 2005). Conjugated polymer that was synthesized by Kumaraswamy et al. (2004) is labelled as a superquencher with its K_{sv} at 7.7 x 10^7 M^{-1}. With its superquenching ability, conjugated polymer was used as sensor to detect protease activity (Kumaraswamy et al., 2004). Conjugated polymer-GNP pair by Fan et al. (2003) has a K_{sv} around 10^{11} M^{-1}. It is several times more efficient than any reported conjugated polymer-quencher pairs and even more efficient than the typical small molecule-dye quencher pairs. Hence, AuNS-TA-ZnS might have the potential to be a biosensor owning to its high K_{sv} value.

Besides, the binding constant, K_b is determined to be 6.7 x 10^{11} M^{-1}. This value appears to be higher than the binding constant of metal(salophen) complexes and its derivatives which are in the range of 10^3 – 10^6 M^{-1} (Ambika et al., 2019; Gurusamy et al., 2022; Rani et al., 2021), implicating AuNS-TA-ZnS bind to BSA better than the free metal complexes.

The number of binding sites, n found is 1.19 which is almost equal to 1. Hence, it can be understood as BSA and AuNS-TA-ZnS formed a complex with 1:1 ratio where AuNS-TA-ZnS binds with BSA at 1 binding site (Naveenraj et al., 2010; X. Shi et al., 2012).

Synchronous fluorescence scanning is a useful technique to allow the detection of weak Tyr fluorescence signal in BSA (Miller, 1983) The microenvironment of Tyr and Trp residues could also be studied with synchronous scanning by setting the wavelength interval, $\Delta\lambda$ at 15 nm and 60 nm respectively.

Figure 4.16 and figure 4.17 illustrate the fluorescence intensity for both Tyr and Trp decreases when the concentration of AuNS-TA-ZnS increases. There is no red-shift or blue-shift observed from the emission wavelength, indicates no change in the hydrophobicity around both Trp and Tyr residues, The folding state of BSA is not affected during its interaction with AuNS-TA-ZnS (J.-h. Shi et al., 2016).

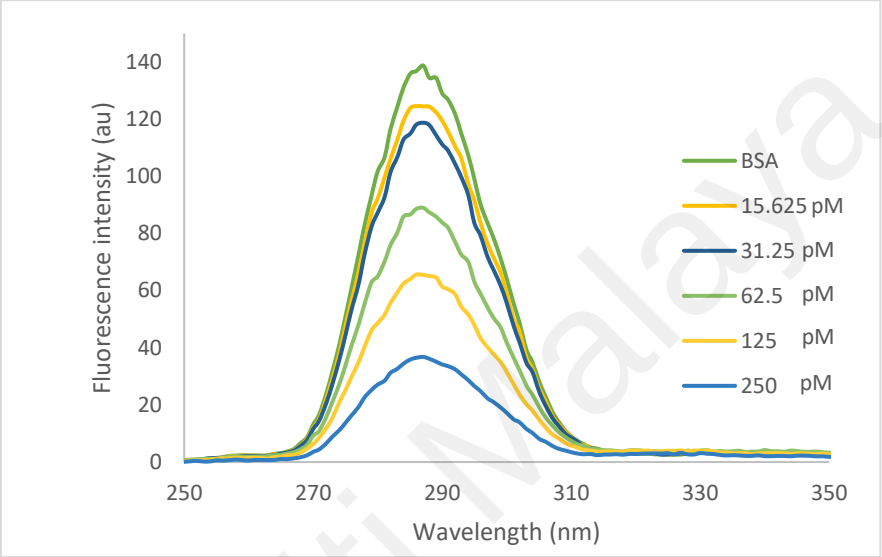

Figure 4.16 Synchronous fluorescence spectra of BSA + AuNS-TA-ZnS in concentration ranging from 0 - 250 pM at Δλ = 15 nm.

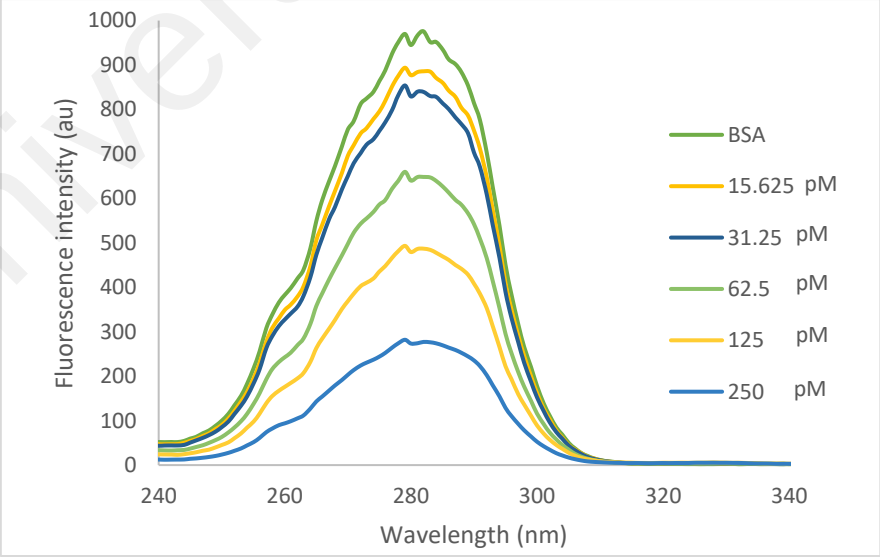

Figure 4.17: Synchronous fluorescence spectra of BSA + AuNS-TA-ZnS in concentration ranging from 0 - 250 pM at Δλ = 60 nm.

4.2.2 BSA Interaction Study via CD

CD is commonly used to elucidate the modifications on the secondary structure of protein when protein interacts with small molecule (Lu et al., 1987). BSA consists 62% of alpha-helices, 13% of beta-sheets, 14% of beta-turns and 11% of random structures (Bourassa et al., 2011). The CD spectrum of BSA at pH 7.4 usually shows two negative minima in the UV region of 208 and 222 nm. These are the characteristic peaks for α-helical configuration of BSA (Buddanavar et al., 2017; Dasgupta et al., 2016). The negative band at 208 nm is due to the exciton splitting of the lowest peptide π - π* transition; while the negative band at 220 nm is due to the peptide n - π* transition (D. M. Rogers et al., 2019).

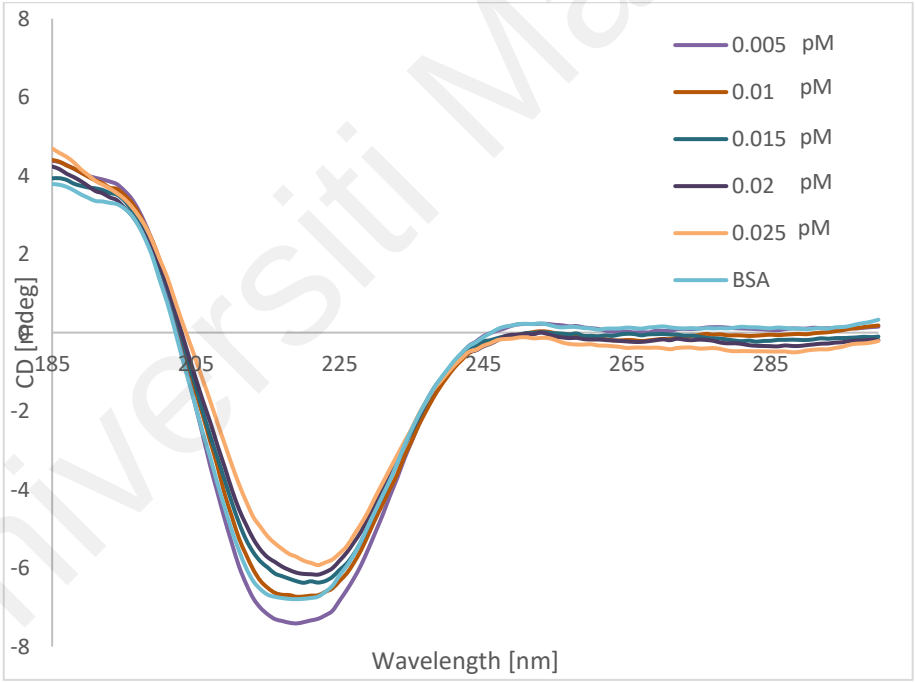

Figure 4.18: CD spectra of BSA interaction with AuNS.

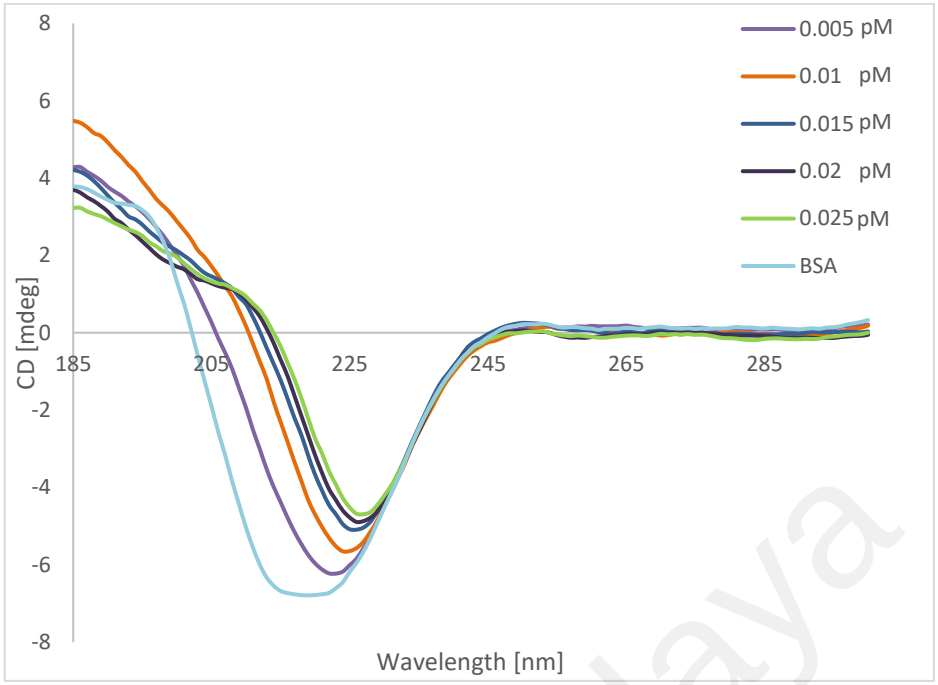

Figure 4.19: CD spectra of BSA interaction with AuNS-TA-ZnS.

From figure 4.18, as the concentration of AuNS increases, the broad negative bands around 208 to 220 nm of the CD spectrum of BSA decrease slightly, which indicates that the intramolecular forces responsible for maintaining the secondary structure is mainly intact in the presence of AuNS. Similar findings were obtained in the interaction of silver nanoparticle with BSA (Dasgupta et al., 2016). From figure 4.19, the intensity of these two bands decreases appreciably with increasing concentration of AuNS-TA-ZnS. This implies significant loss of BSA's α-helicity. The decreased content of the α-helical structure indicates that AuNS-TA-ZnS nanoparticles might have bound with the amino acid residues in the main polypeptide chain and interact with the hydrogen bonding networks of the protein (Shaikh et al., 2007; Sood et al., 2018).

4.2.3 20S Mouse Proteasome Inhibition Assay

Proteasome is known as a protein responsible for degrading damaged or short-lived intracellular proteins in mammalian cells via proteolysis (Kisselev et al., 2003). Inhibition

of proteasome may help to overcome drug resistance (Patra et al., 2015, Kucuksayan et al., 2021) and stimulate apoptosis in cancer cells (Kucuksayan et al., 2021).

After 24 hours incubation of AuNS-TA-ZnS with 20S mouse proteasome, the proteolytic sites which were not inhibited by AuNS-TA-ZnS bound with their respective fluorogenic peptide substrate. Proteolysis of these peptide substrates released AMC (7-amino-4-methylcoumarin) units which emitted fluorescence that is used to quantify the proteolytic activities at each site.

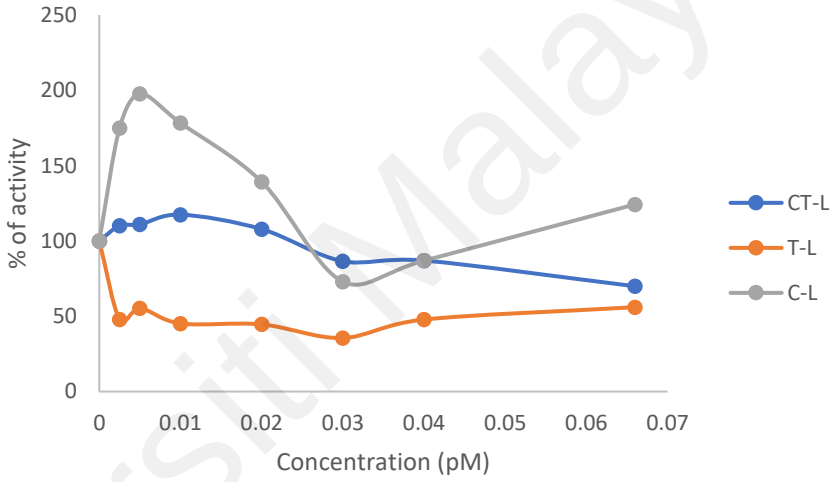

Figure 4.20: Proteolytic activity (%) of Chymotrypsin-like (CT-L) site, Trypsin-like (T-L) site and Caspase-like (C-L) site upon treatment with AuNS-TA-ZnS

As shown in figure 4.20, the proteolytic activity at Trypsin-like (T-L) site drops below 50% at 2 x 10^{-3} pM. This suggests that AuNS-Ta-ZnS may be a specific inhibitor for the T-L site. As Kisselev et al. (2003) and Mirabella et al. (2011) have reported that different proteolytic sites have different specificities depending on their respective binding pockets.

For the chymotrypsin-like (CT-L) site, upon reaching treatment concentration of 0.01 pM, the proteolytic activity decreases in a dose-dependent manner. At 0.066 pM the proteolytic activity decreases to 70%. At the Caspase-like (C-L) site, the interaction of AuNS-TA-ZnS with the site shows temporary reversibility (Mirabella et al., 2011). The

proteolytic activity was enhanced for one-fold at 0.005 pM and decreased gradually to 70% at 0.032 pM before recovering at a higher concentration.

With AuNS-TA-ZnS being an inhibitor specific to the T-L site it might be an efficient cancer drugs. This is due to Mirabella et al. (2011) found that cytotoxicity of inhibitors was correlated with the inhibition of T-L site in most multiple myeloma cell lines. In 2009, Britton et al. discovered that co-inhibition of T-L site and CT-L site would give a higher cytotoxicity level than inhibiting CT-L site solely. The study suggests T-L site should be made as a co-target for anticancer agents, where AuNS-TA-ZnS might be a potential candidate. Besides, AuNS-TA-ZnS have antiprotozoal potential as protozoal proteasome shows high T-L activity; while mammalian (rat) proteasome exhibits low T-L activity (Hua et al., 1996).

4.3 Biological studies

4.3.1 Cell viability assay

In the cell viability assay, growth inhibitory effect of AuNS, AuNS-TA, AuNS-TA-ZnS and ZnS were studied on human breast cancer cells MDA-MB-231, MDA-MB-468, MCF-7, and human intestinal cancer cell Caco-2 for 48 hours. The percentage of cell viability at different treatment concentrations are shown in figure 4.21 – figure 4.24 and the IC_{50} values are tabulated in Table 4.4.

Table 4.4: IC_{50} of AuNS-TA-ZnS and ZnS on various cell lines.

Compounds	IC_{50}			
	MCF-7	MDA-MB-231	MDA-MB-468	Caco2
AuNS-TA-ZnS	565 pM	510 pM	530 pM	405 pM
ZnS	60 µM	42.3 µM	41.5 µM	42 µM

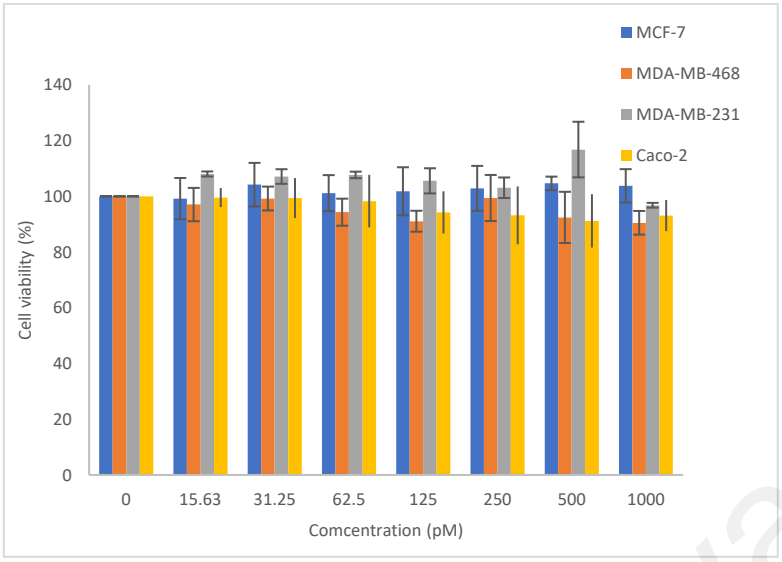

Figure 4.21: Cell viability of various cell lines after 48 hours treatment with AuNS

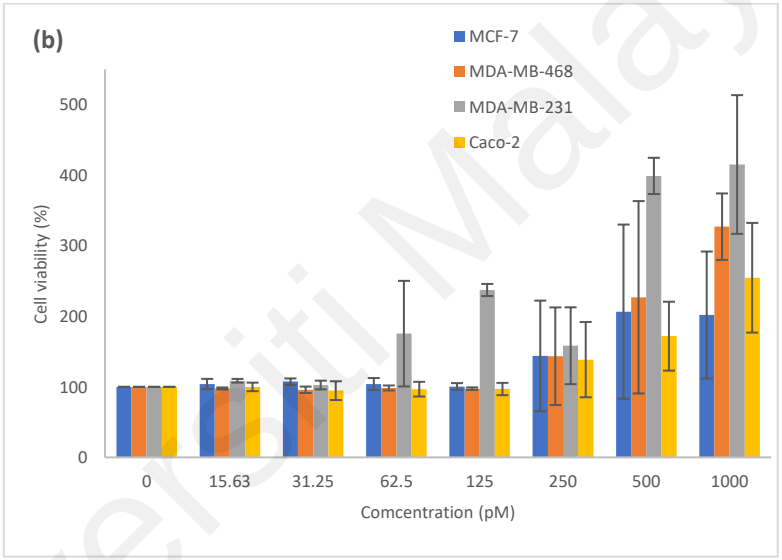

Figure 4.22: Cell viability of various cell lines after 48 hours treatment with AuNS-TA.

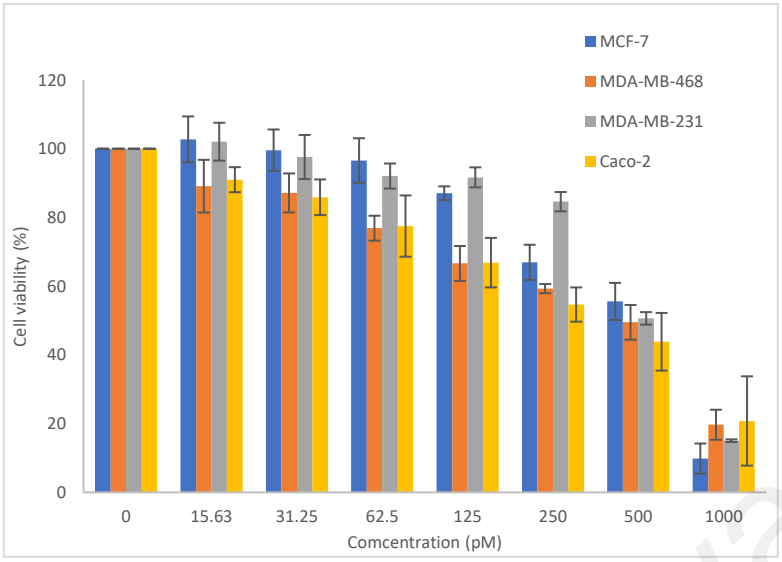

Figure 4.23: Cell viability of various cell lines after 48 hours treatment with AuNS-TA-ZnS.

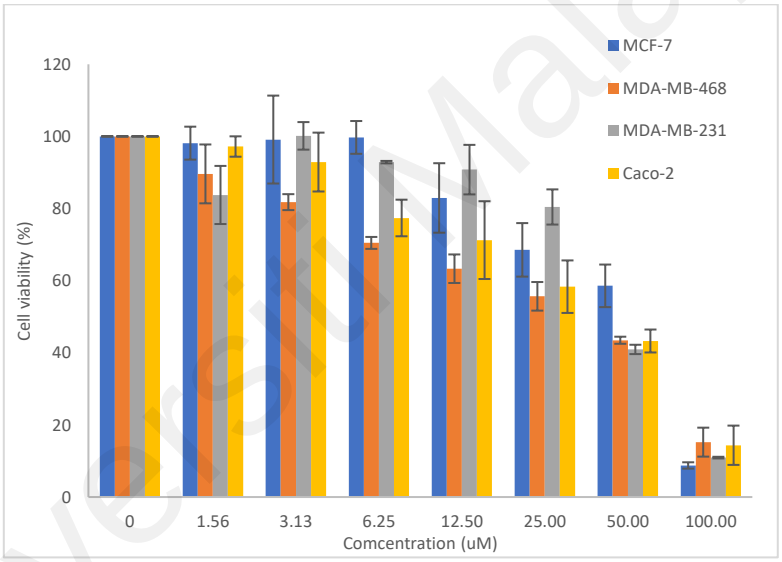

Figure 4.24: Cell viability of various cell lines after 48 hours treatment with ZnS

AuNS does not show any growth inhibition activity; while AuNS-TA shows cell proliferation activities for all the four tested cell lines when the treatment concentration was increased to 250 pM and beyond. This could be due to TA's antioxidative property (Packer et al., 1997) and its ability to promote cell proliferation (Leu et al., 2012).

Both of the treatments with AuNS-TA-ZnS and ZnS show growth inhibition activities. However, the IC_{50} values of AuNS-TA-ZnS for all the tested cell lines are within 400 – 570 pM, while the IC_{50} values of ZnS range between 40 – 60 µM. This signifies that AuNS-TA-ZnS is more cytotoxic when compared to unconjugated ZnS.

The result from 20S mouse proteasome inhibition study suggests that the cytotoxicity of AuNS-TA-ZnS might be due to its ability to inhibit specifically at the T-L site. Besides, high surface to volume ratio of the nanoparticle is one of the factors that contribute to the enhancement of cytotoxicity in AuNS-TA-ZnS, as more free ZnS molecules are able to bound on a single nanoparticle.

Another advantage that nanoparticles possess is the engagement of endocytosis pathway to deliver drugs into the cells which increases the effectiveness of drug delivery (Ahn et al., 2013; Siew et al., 2012). Upon entering the cells, the disulfide bonds of TA can be reduced easily by the cells into dihydrolipoic acid (Handelman et al., 1994, Saito et al., 2003). This helps to release ZnS from the surface of AuNS-TA-ZnS and increase the bioavailability of ZnS in cells. Hence, this could also be a reason of AuNS-TA-ZnS being more potent than ZnS.

4.3.2 Intracellular Reactive Oxygen Species (ROS) Assay

ROS are mainly generated in the mitochondria as products from cellular metabolism (Valko et al., 2004). Cancer cells could be killed by inducing a high level of ROS in the cells which surpasses its lethal level and leads to an irreversible oxidative damage to the cells (Zhu et al., 2014). AuNS-TA-ZnS are able to generate a similar level of ROS as ZnS at a relatively lower concentration which might be due to the possibilities discussed in chapter 4.3.1.

Table 4.5: Fold change of ROS generated in each cell line at various concentrations.

		Fold Change of ROS	
		MCF-7	MDA-MB-231
Concentration of AuNS-TA-ZnS (pM)	250	1.0134 +/- 0.1516	0.7578 +/- 0.0316
	125	0.8410 +/- 0.0061	0.9406 +/- 0.0963

Table 4.5, continued

		Fold Change of ROS	
		MCF-7	MDA-MB-231
Concentration of AuNS-TA-ZnS (pM)	62.5	0.7101 +/- 0.1045	1.2243 +/- 0.0216
Concentration of ZnS (uM)	25	1.2211 +/- 0.0473	0.8921 +/- 0.0064
	12.5	0.9579 +/- 0.1074	0.7088 +/- 0.0286
	6.25	0.9585 +/- 0.0801	1.3631 +/- 0.2274

In MCF-7 cell line, both AuNS-TA-ZnS (figure 4.25) and ZnS (figure 4.26) induced ROS in a dose dependent manner. An increase in the concentration of test compound stimulated the production of more ROS. When ROS exceeded the cellular level of ROS, it may damage the nucleic acids, protein, membranes and organelles, leading to cell death (Redza-Dutordoir et al., 2016). For MDA-MB-231 cell line, cells treated with AuNS-TA-ZnS generated ROS at a reverse dose dependent manner despite its dose dependent cytotoxicity. This suggests that the cell death of MDA-MB-231 may not follow the ROS-dependent pathway.

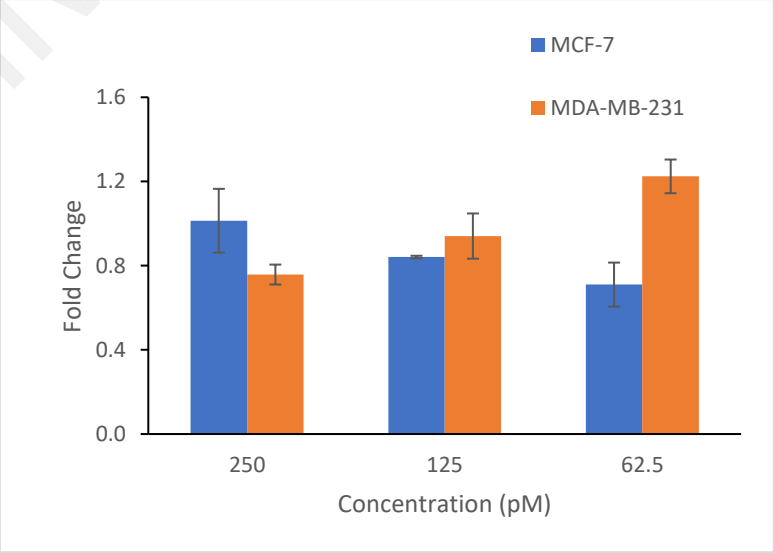

Figure 4.25: Fold Change of ROS in MCF-7 and MDA-MB-231 after treatment with AuNS-TA-ZnS.

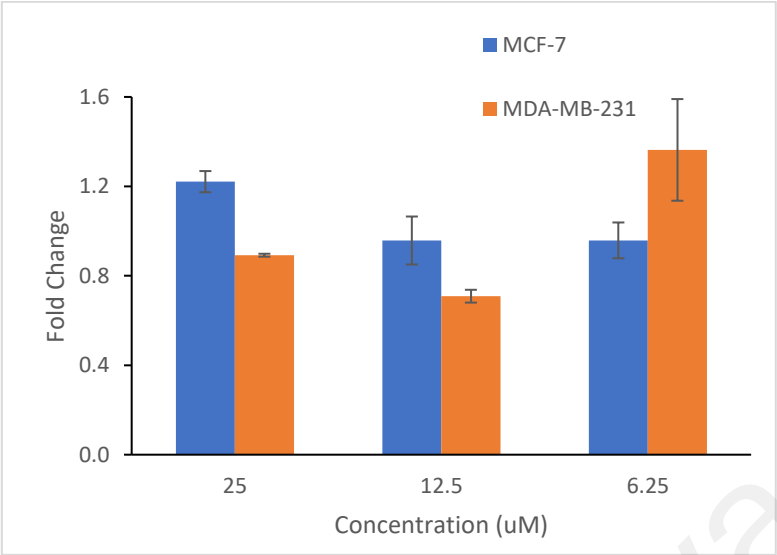

Figure 4.26: Fold Change of ROS in MCF-7 and MDA-MB-231 after treatment with ZnS.

4.3.3 TEER Measurement

The availability of orally taken drug is highly dependent on the quality of the gastrointestinal tract's barrier function (Srinivasan et al., 2015). In this study, we differentiated the human colon cancer cells, Caco-2 cells to mimic the intestinal barrier which controls the passage of macro molecules, water, solutes and ions in our gastrointestinal tract (Gao et al., 2017). As mentioned by Guha et al. (2021) and Artursson et al. (2001), there are four main routes that can be used to transport nutrients and drugs across Caco-2 cells namely i) passive paracellular route via the tight junction complexes, ii) active transport by transporter iii) transcytosis and iv) passive transcellular route through the cell.

In this experiment, we have studied the passive paracellular route. A polarised monolayer with intercellular tight junction was formed upon differentiation. The tight junction consists of several proteins such as claudin and occuludin which regulate the diffusion or transport process through intracellular pathway (Benson et al., 2013). By using this model, studies have shown that different nanoparticles can be transported across the epithelial monolayer (Chai et al., 2016; Fröhlich et al., 2012).

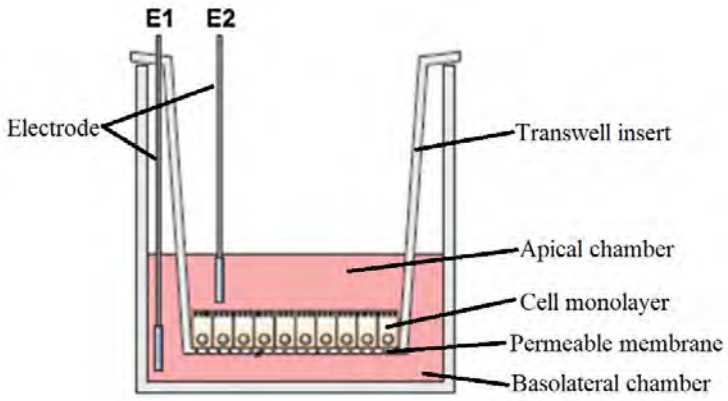

Figure 4.27: Setup of cell permeability study via TEER measurement. (Adapted from Benson et al., 2013)

The integrity of tight junction could be evaluated by measuring the TEER across the monolayer (Benson et al., 2013). It is a non-invasive method and suitable for continuous monitoring of the barrier integrity (Srinivasan et al., 2015).

AuNS-TA-ZnS and ZnS were treated to the differentiated Caco-2 cells by releasing the drug into the apical chamber at concentrations lower than their IC_{50}. Prior to the treatment, initial TEER value in each well was measured and the values were between 55 – 60 Ω cm^2. TEER reading was monitored every 30 minutes for 3 hours and the percent change from their initial TEER was tabulated and shown in figure 4.28.

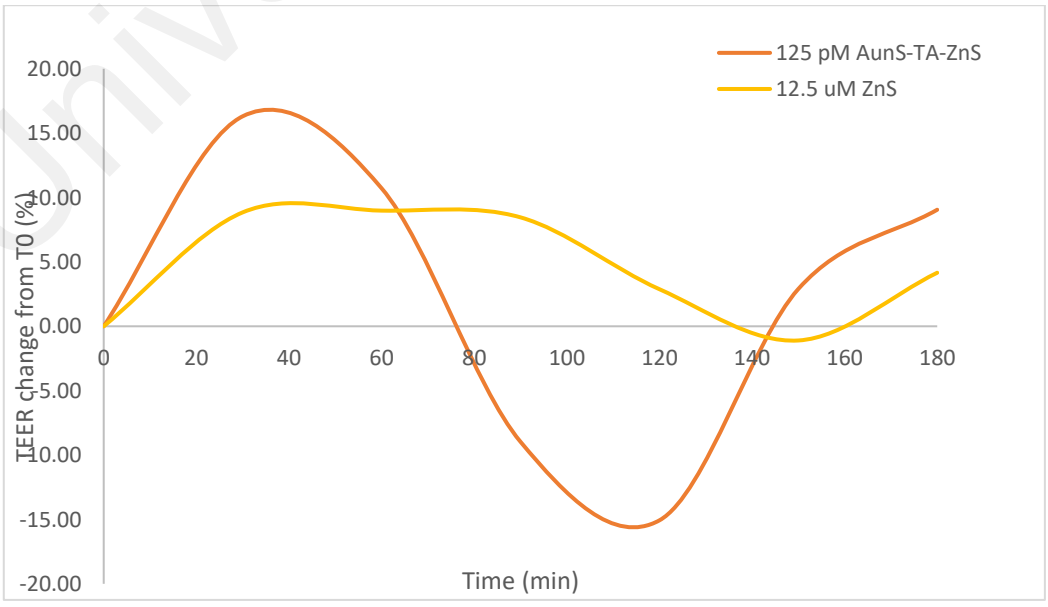

Figure 4.28: TEER measurement of Caco-2 cells for 3 hours.

An increment in TEER at the beginning of the treatment is observed for both AuNS-TA-ZnS and ZnS which may be due to cell swelling (Chapman et al., 2012). The TEER value for chamber treated with AuNS-TA-ZnS decreased below its initial TEER value at the 75th minute. This implicates that the integrity of tight junction was disrupted (Chapman et al., 2012; Gao et al., 2017), offering drugs a monolayer with higher permeability to pass through (Amin et al., 2009; Franke et al., 1999; Hasegawa et al., 1999).

The TEER value kept decreasing to 15.5% lesser than its initial TEER before changing its trend to increasing which indicates that the barrier has started to recover (Wagner et al., 2010). At this stage, barrier integrity started to strengthen and paracellular permeability across the Caco-2 monolayer decreased (N. Khan et al., 2017). This observation resembles the finding from Benson et al. (2013) where poly(butyl)cyanoacrylate nanoparticles was able to open the blood-brain barrier temporarily. For ZnS, the TEER value falls below its initial TEER reading at the 136th minute and reached a maximum change of 1% before recovering.

It is also observed that treatment with AuNS-TA-ZnS offers a longer window (70 minutes) than ZnS (24 minutes) for the drugs to permeate through the Caco-2 monolayer. Besides, the percentage change in between the initial TEER value and the minimum TEER value for AuNS-TA-ZnS is greater than ZnS. This suggests that AuNS-TA-ZnS could induce a weaker barrier integrity and allow more drugs to pass through the cell monolayer when compared to ZnS.

CHAPTER 5: CONCLUSION

The formation of the inorganic gold nanosphere-thioctic acid-Zn(salophen) conjugate (AuNS-TA-ZnS) is supported by FTIR spectra and UV-vis. The conjugate exhibits SPR at 521 nm. ZnS has a stronger fluorescence than its ligand; however, the fluorescence of ZnS was quenched after the formation of AuNS-TA-ZnS. This was due to the fluorescence emission of ZnS experienced non-radiative decay, instead of having the MEF effect which will enhance the fluorescence of ZnS upon conjugating with AuNS-TA.

TEM images confirm the nanoparticles are spherical in shape. The diameter of AuNS is 14.97 nm while AuNS-TA-ZnS has an average diameter of 17.73 nm. DLS analysis suggests that the size of the AuNS nanoparticles grew larger after forming conjugates with ZnS; however, it appeared larger than those measured with TEM. From zeta potential analysis, it is observed that AuNS-TA-ZnS is less stable than the unconjugated AuNS. This leads to the aggregation of AuNS-TA-ZnS which caused the excessive scattering that results to an overestimation in size. The loading of ZnS on AuNS-TA was calculated from ICP-MS where 1785 ZnS molecules is found to bound on a single AuNS-TA.

AuNS-TA-ZnS bounds to BSA at one site with high affinity. Synchronous fluorescence scanning of the BSA and AuNS-TA-ZnS mixture shows that the tertiary conformation of BSA was not affected by AuNS-TA-ZnS; while CD spectral analysis shows that AuNS-TA-ZnS interacted with the secondary structure of BSA.

Study with another protein, 20S proteasome indicates that AuNS-TA-ZnS inhibits proteolytic activities at the T-L site more selectively than the other two proteolytic sites of 20S proteasome.

AuNS does not possess cytotoxic effect on the MCF-7, MDA-MB-231, MDA-MB-468 and Caco-2 cell lines. On the other hand, AuNS-TA-ZnS are more potent than the unconjugated ZnS. Both ZnS and AuNS-TA-ZnS were able to generate ROS when tested on MCF-7 and MDA-MB-231 cell lines, with AuNS-TA-ZnS induced ROS at a concentration of pM while ZnS at a concentration of μM. By monitoring TEER of the Caco-2 cell monolayer, AuNS-TA-ZnS are found to be more able to weakened the monolayer's integrity and might allow more drugs to permeate through the cell monolayer when compared to ZnS.

5.1 Suggestion

It was understood that the enhancing and quenching of the fluorophore's fluorescent by GNP is highly depending on the distance between them. Thus, conjugating ZnS and gold nanosphere by using a longer linker, for example thiolated-polyethylene glycol (PEG) may help the conjugates achieve metal enhanced fluorescent (MEF) effect (Chen et al., 2007; Dulkeith et al., 2005; Reineck et al., 2013). By combining with the ability of AuNS acting as a drug delivery scaffold with high payload, this may allow future conjugates to serve as theranostic drugs for cancer cell imaging and therapy.

REFERENCES

Abdel-Haleem, F. M., Badr, I. H. A., & Rizk, M. S. (2016). Potentiometric anion selectivity and analytical applications of polymer membrane electrodes based on novel Mn(III)- and Mn(IV)-Salophen complexes. *Electroanalysis, 28*(12), 2922-2929.

Achyuthan, K. E., Bergstedt, T. S., Chen, L., Jones, R. M., Kumaraswamy, S., Kushon, S. A., . . . Whitten, D. G. (2005). Fluorescence superquenching of conjugated polyelectrolytes: Applications for biosensing and drug discovery. *Journal of Materials Chemistry, 15*(27-28), 2648-2656.

Ahn, S., Seo, E., Kim, K., & Lee, S. J. (2013). Controlled cellular uptake and drug efficacy of nanotherapeutics. *Scientific Reports, 3*(1), Article#1997.

Alanazi, F. K., Radwan, A. A., & Alsarra, I. A. (2010). Biopharmaceutical applications of nanogold. *Saudi Pharmaceutical Journal : SPJ : The Official Publication of the Saudi Pharmaceutical Society, 18*(4), 179-193.

Ambika, S., Manojkumar, Y., Arunachalam, S., Gowdhami, B., Meenakshi Sundaram, K. K., Solomon, R. V., . . . Sundararaman, M. (2019). Biomolecular interaction, anti-cancer and anti-angiogenic properties of cobalt(III) Schiff base complexes. *Scientific Reports, 9*(1), Article#2721.

Amendola, V., Pilot, R., Frasconi, M., Maragò, O. M., & Iatì, M. A. (2017). Surface plasmon resonance in gold nanoparticles: A review. *Journal of Physics: Condensed Matter, 29*(20), Article#203002.

Amin, R., Artmann, T. A., Artmann, G., Lazarovici, P., & Lelkes, P. I. (2009). *Permeability of an In Vitro Model of Blood Brain Barrier (BBB).* Paper presented at the 13th International Conference on Biomedical Engineering, Berlin, Heidelberg.

Anger, P., Bharadwaj, P., & Novotny, L. (2006). Enhancement and quenching of single-molecule fluorescence. *Physical Review Letters, 96*(11), Article#113002.

Ansari, K. I., Kasiri, S., Grant, J. D., & Mandal, S. S. (2009). Apoptosis and anti-tumour activities of manganese(iii)-salen and -salphen complexes. *Dalton Transactions*(40), 8525-8531.

Artursson, P., Palm, K., & Luthman, K. (2001). Caco-2 monolayers in experimental and theoretical predictions of drug transport. *Advanced Drug Delivery Reviews, 46*(1-3), 27-43.

Arunachalam, K. D., Annamalai, S. K., & Hari, S. (2013). One-step green synthesis and characterization of leaf extract-mediated biocompatible silver and gold nanoparticles from Memecylon umbellatum. *International Journal of Nanomedicine, 8*, 1307-1315.

Aryal, S., B, K. C. R., Dharmaraj, N., Bhattarai, N., Kim, C. H., & Kim, H. Y. (2006). Spectroscopic identification of S-Au interaction in cysteine capped gold

nanoparticles. *Spectrochimica Acta A: Molecular and Biomolecular Spectroscopy, 63*(1), 160-163.

Asadi, Z., Asadi, M., & Shorkaei, M. R. (2016). Synthesis, characterization and DFT study of new water-soluble aluminum(III), gallium(III) and indium(III) Schiff base complexes: Effect of metal on the binding propensity with bovine serum albumin in water. *Journal of the Iranian Chemical Society, 13*(3), 429-442.

Asadi, Z., Haddadi, E., & Sedaghat, M. (2017). Substitution of PPh3+ as a lipophilic cation on new water-soluble Co(II) and Zn(II) Schiff base complexes: Effect of central metal and substitutional group of ligand on DNA-complex interaction. *Journal of Photochemistry and Photobiology A: Chemistry, 337*, 140-150.

Bahramian, B., Mirkhani, V., Moghadam, M., & Amin, A. H. (2006). Water-soluble manganese(III) salen complex as a mild and selective catalyst for oxidation of alcohols. *Applied Catalysis A: General, 315*, 52-57.

Beloglazkina, E. K., Majouga, A. G., Romashkina, R. B., Zyk, N. V., & Zefirov, N. S. (2012). Gold nanoparticles modified with coordination compounds of metals: Synthesis and application. *Russian Chemical Reviews, 81*(1), 65-90.

Benson, K., Cramer, S., & Galla, H.-J. (2013). Impedance-based cell monitoring: Barrier properties and beyond. *Fluids and Barriers of the CNS, 10*(1), Article#5.

Bhattacharjee, S. (2016). DLS and zeta potential - What they are and what they are not? *Journal of Controlled Release, 235*, 337-351.

Bonoiu, A. C., Mahajan, S. D., Ding, H., Roy, I., Yong, K. T., Kumar, R., . . . Prasad, P. N. (2009). Nanotechnology approach for drug addiction therapy: Gene silencing using delivery of gold nanorod-siRNA nanoplex in dopaminergic neurons. *Proceedings of the National Academy of Sciences of the United States of America, 106*(14), 5546-5550.

Bourassa, P., Hasni, I., & Tajmir-Riahi, H. A. (2011). Folic acid complexes with human and bovine serum albumins. *Food Chemistry, 129*(3), 1148-1155.

Brissos, R., Ramos, D., Lima, J. C., Mihan, F. Y., Borràs, M., de Lapuente, J., . . . Rodríguez, L. (2013). Luminescent zinc salophen derivatives: Cytotoxicity assessment and action mechanism studies. *New Journal of Chemistry, 37*(4), 1046-1055.

Britton, M., Lucas, M. M., Downey, S. L., Screen, M., Pletnev, A. A., Verdoes, M., . . . Kisselev, A. F. (2009). Selective inhibitor of proteasome's caspase-like sites sensitizes cells to specific inhibition of chymotrypsin-like sites. *Chemistry & Biology, 16*(12), 1278-1289.

Bruce B. Weiner, W. W. T., David Fairhurst. (1993). *Zeta Potential: A New Approach*. Paper presented at the Canadian Mineral Analysts Meeting, Winnipeg, Manitoba, Canada.

Brust, M., Walker, M., Bethell, D., Schiffrin, D. J., & Whyman, R. (1994). Synthesis of thiol-derivatised gold nanoparticles in a two-phase Liquid–Liquid system. *Journal of the Chemical Society, Chemical Communications*(7), 801-802.

Buddanavar, A. T., & Nandibewoor, S. T. (2017). Multi-spectroscopic characterization of bovine serum albumin upon interaction with atomoxetine. *Journal of Pharmaceutical Analysis, 7*(3), 148-155.

Cano, M., Rodríguez, L., Lima, J. C., Pina, F., Dalla Cort, A., Pasquini, C., & Schiaffino, L. (2009). Specific supramolecular interactions between Zn2+-salophen complexes and biologically relevant anions. *Inorganic Chemistry, 48*(13), 6229-6235.

Carnovale, C., Bryant, G., Shukla, R., & Bansal, V. (2016). Size, shape and surface chemistry of nano-gold dictate its cellular interactions, uptake and toxicity. *Progress in Materials Science, 83*, 152-190.

Carter, D. C., & Ho, J. X. (1994). Structure of serum albumin. *Advances in Protein Chemistry, 45*, 153-203.

Chai, G.-H., Xu, Y., Chen, S.-Q., Cheng, B., Hu, F.-Q., You, J., . . . Yuan, H. (2016). Transport mechanisms of solid lipid nanoparticles across Caco-2 cell monolayers and their related cytotoxicology. *ACS Applied Materials & Interfaces, 8*(9), 5929-5940.

Chandran, S. P., Chaudhary, M., Pasricha, R., Ahmad, A., & Sastry, M. (2006). Synthesis of gold nanotriangles and silver nanoparticles using aloevera plant extract. *Biotechnology Progress, 22*(2), 577-583.

Chapman, J. C., Liu, Y., Zhu, L., & Rhoads, J. M. (2012). Arginine and citrulline protect intestinal cell monolayer tight junctions from hypoxia-induced injury in piglets. *Pediatric Research, 72*(6), 576-582.

Chen, Y., Munechika, K., & Ginger, D. S. (2007). Dependence of fluorescence intensity on the spectral overlap between fluorophores and plasmon resonant single silver nanoparticles. *Nano Letters, 7*(3), 690-696.

Comby, S., & Gunnlaugsson, T. (2011). Luminescent lanthanide-functionalized gold noparticles: Exploiting the interaction with bovine serum albumin for potential sensing applications. *ACS Nano, 5*(9), 7184-7197.

Connor, E. E., Mwamuka, J., Gole, A., Murphy, C. J., & Wyatt, M. D. (2005). Gold nanoparticles are taken up by human cells but do not cause acute cytotoxicity. *Small, 1*(3), 325-327.

Craig, G. E., Brown, S. D., Lamprou, D. A., Graham, D., & Wheate, N. J. (2012). Cisplatin-tethered gold nanoparticles that exhibit enhanced reproducibility, drug loading, and stability: A step closer to pharmaceutical approval? *Inorganic Chemistry, 51*(6), 3490-3497.

Cui, T., Liang, J.-J., Chen, H., Geng, D.-D., Jiao, L., Yang, J.-Y., . . . Ding, Y. (2017). Performance of Doxorubicin-conjugated gold nanoparticles: Regulation of drug location. *ACS Applied Materials & Interfaces, 9*(10), 8569-8580.

Dalla Cort, A., De Bernardin, P., & Schiaffino, L. (2009). A new water soluble Zn-salophen derivative as a receptor for alpha-aminoacids: Unexpected chiral discrimination. *Chirality, 21*(1), 104-109.

Dalla Cort, A., Mandolini, L., & Schiaffino, L. (2005). Exclusive transition state stabilization in the supramolecular catalysis of Diels–Alder reaction by a uranyl salophen complex. *Chemical Communications*(30), 3867-3869.

Danaei, M., Dehghankhold, M., Ataei, S., Hasanzadeh Davarani, F., Javanmard, R., Dokhani, A., . . . Mozafari, M. R. (2018). Impact of particle size and polydispersity index on the clinical applications of lipidic nanocarrier systems. *Pharmaceutics, 10*(2), Article#57.

Dasgupta, N., Ranjan, S., Patra, D., Srivastava, P., Kumar, A., & Ramalingam, C. (2016). Bovine serum albumin interacts with silver nanoparticles with a "side-on" or "end on" conformation. *Chemico-Biological Interactions, 253*, 100-111.

Decortes, A., Martínez Belmonte, M., Benet-Buchholz, J., & Kleij, A. W. (2010). Efficient carbonate synthesis under mild conditions through cycloaddition of carbon dioxide to oxiranes using a Zn(salphen) catalyst. *Chemical Communications, 46*(25), 4580-4582.

Dell'Orco, D., Lundqvist, M., Linse, S., & Cedervall, T. (2014). Mathematical modeling of the protein corona: implications for nanoparticulate delivery systems. *Nanomedicine, 9*(6), 851-858.

Deng, Y., Wang, C. C., Choy, K. W., Du, Q., Chen, J., Wang, Q., . . . Tang, T. (2014). Therapeutic potentials of gene silencing by RNA interference: Principles, challenges, and new strategies. *Gene, 538*(2), 217-227.

Doctrow, S. R., Huffman, K., Marcus, C. B., Tocco, G., Malfroy, E., Adinolfi, C. A., . . . Malfroy, B. (2002). Salen-manganese complexes as catalytic scavengers of hydrogen peroxide and cytoprotective agents: Structure-activity relationship studies. *Journal of Medicinal Chemistry, 45*(20), 4549-4558.

Dong, W.-K., Xing, S.-J., Sun, Y.-X., Zhao, L., Chai, L.-Q., & Gao, X.-H. (2012). An unprecedented tetranuclear Zn(II) complex with an unsymmetric Salen-type bisoxime ligand: Synthesis, crystal structure, and spectral properties. *Journal of Coordination Chemistry, 65*(7), 1212-1220.

Dreaden, E. C., Mackey, M. A., Huang, X., Kang, B., & El-Sayed, M. A. (2011). Beating cancer in multiple ways using nanogold. *Chemical Society Reviews, 40*(7), 3391-3404.

Duarte, S., Carle, G., Faneca, H., de Lima, M. C., & Pierrefite-Carle, V. (2012). Suicide gene therapy in cancer: Where do we stand now? *Cancer Letters, 324*(2), 160-170.

Dube, E., Oluwole, D. O., Nwaji, N., & Nyokong, T. (2018). Glycosylated zinc phthalocyanine-gold nanoparticle conjugates for photodynamic therapy: Effect of nanoparticle shape. *Spectrochimica Acta Part A: Molecular and Biomolecular Spectroscopy, 203*, 85-95.

Dulkeith, E., Ringler, M., Klar, T. A., Feldmann, J., Muñoz Javier, A., & Parak, W. J. (2005). Gold nanoparticles quench fluorescence by phase induced radiative rate suppression. *Nano Letters, 5*(4), 585-589.

Dumur, F., Contal, E., Wantz, G., & Gigmes, D. (2014). Photoluminescence of zinc complexes: Easily tunable optical properties by variation of the bridge between the imido groups of Schiff base ligands. *European Journal of Inorganic Chemistry, 2014*(25), 4186-4198.

Dumur, F., Dumas, E., & Mayer, C. R. (2020). Functionalization of gold nanoparticles by inorganic entities. *Nanomaterials, 10*(3), Article#548.

Ebrahimipour, S. Y., Mohamadi, M., Torkzadeh Mahani, M., Simpson, J., Mague, J. T., & Sheikhshoaei, I. (2017). Synthesis and structure elucidation of novel salophen-based dioxo-uranium(VI) complexes: In-vitro and in-silico studies of their DNA/BSA-binding properties and anticancer activity. *European Journal of Medicinal Chemistry, 140*, 172-186.

Egea, E., Mendoza, D., Garavito, G., Saavedra, S., Gómez, H., & Sanjuan, M. (2019). Nanogold - IgY antibodies. An immunoconjugated for the detection of house dust mite (Dermatophagoides) allergens. *Journal of Immunological Methods, 464*, 15-21.

El-Medani, S. M., Ali, O. A. M., & Ramadan, R. M. (2005). Photochemical reactions of group 6 metal carbonyls with N-salicylidene-2-hydroxyaniline and bis-(salicylaldehyde)phenylenediimine. *Journal of Molecular Structure, 738*(1), 171-177.

England, C. G., Miller, M. C., Kuttan, A., Trent, J. O., & Frieboes, H. B. (2015). Release kinetics of paclitaxel and cisplatin from two and three layered gold nanoparticles. *European Journal of Pharmaceutics and Biopharmaceutics, 92*, 120-129.

Eustis, S., & El-Sayed, M. A. (2006). Why gold nanoparticles are more precious than pretty gold: Noble metal surface plasmon resonance and its enhancement of the radiative and nonradiative properties of nanocrystals of different shapes. *Chemical Society Reviews, 35*(3), 209-217.

Fan, C., Wang, S., Hong, J. W., Bazan, G. C., Plaxco, K. W., & Heeger, A. J. (2003). Beyond superquenching: Hyper-efficient energy transfer from conjugated polymers to gold nanoparticles. *Proceedings of the National Academy of Sciences, 100*(11), 6297-6301.

Franke, H., Galla, H. J., & Beuckmann, C. T. (1999). An improved low-permeability in vitro-model of the blood-brain barrier: Transport studies on retinoids, sucrose, haloperidol, caffeine and mannitol. *Brain Research, 818*(1), 65-71.

Fröhlich, E., & Roblegg, E. (2012). Models for oral uptake of nanoparticles in consumer products. *Toxicology, 291*(1-3), 10-17.

Fu, X.-H. (2007). Electrochemical immunoassay for carbohydrate antigen-125 based on polythionine and gold hollow microspheres modified glassy carbon electrodes. *Electroanalysis, 19*(17), 1831-1839.

Fujita, Y., Kuwano, K., & Ochiya, T. (2015). Development of small RNA delivery systems for lung cancer therapy. *International Journal of Molecular Sciences, 16*(3), 5254-5270.

Ganjali, M. R., Shirvani-Arani, S., Norouzi, P., Rezapour, M., & Salavati-Niasari, M. (2004). Novel nitrite membrane sensor based on cobalt(II) salophen for selective monitoring of nitrite ions in biological samples. *Microchimica Acta, 146*(1), 35-41.

Gao, Y., Li, S., Wang, J., Luo, C., Zhao, S., & Zheng, N. (2017). Modulation of intestinal epithelial permeability in differentiated Caco-2 cells exposed to Aflatoxin M1 and Ochratoxin A individually or collectively. *Toxins, 10*(1), Article#13.

Garle, M. J., Fentem, J. H., & Fry, J. R. (1994). In vitro cytotoxicity tests for the prediction of acute toxicity in vivo. *Toxicology in Vitro, 8*(6), 1303-1312.

Ghisaidoobe, A. B. T., & Chung, S. J. (2014). Intrinsic tryptophan fluorescence in the detection and analysis of proteins: A focus on Förster resonance energy transfer techniques. *International Journal of Molecular Sciences, 15*(12), 22518-22538.

Gomathi Sankareswari, V., Vinod, D., Mahalakshmi, A., Alamelu, M., Kumaresan, G., Ramaraj, R., & Rajagopal, S. (2014). Interaction of oxovanadium(iv)–salphen complexes with bovine serum albumin and their cytotoxicity against cancer. *Dalton Transactions, 43*(8), 3260-3272.

Goodman, C. M., McCusker, C. D., Yilmaz, T., & Rotello, V. M. (2004). Toxicity of gold nanoparticles functionalized with cationic and anionic side chains. *Bioconjugate Chemistry, 15*(4), 897-900.

Guha, S., Alvarez, S., & Majumder, K. (2021). Transport of dietary anti-inflammatory peptide, γ-glutamyl valine (γ-EV), across the intestinal Caco-2 monolayer. *Nutrients, 13*(5), Article#1448.

Gurusamy, S., Krishnaveni, K., Sankarganesh, M., Nandini Asha, R., & Mathavan, A. (2022). Synthesis, characterization, DNA interaction, BSA/HSA binding activities of VO(IV), Cu(II) and Zn(II) Schiff base complexes and its molecular docking with biomolecules. *Journal of Molecular Liquids, 345*, Article#117045.

Gusev, A., Shul'gin, V., Braga, E., Zamnius, E., Kryukova, M., & Linert, W. (2020). Luminescent properties of Zn complexes based on tetradentate N2O2-donor pyrazolone Schiff bases. *Dyes and Pigments, 183*, Article#108626.

Haak, R. M., Wezenberg, S. J., & Kleij, A. W. (2010). Cooperative multimetallic catalysis using metallosalens. *Chemical Communications, 46*(16), 2713-2723.

Haiss, W., Thanh, N. T. K., Aveyard, J., & Fernig, D. G. (2007). Determination of size and concentration of gold nanoparticles from UV−Vis spectra. *Analytical Chemistry, 79*(11), 4215-4221.

Halle, W. (2003). The registry of cytotoxicity: Toxicity testing in cell cultures to predict acute toxicity (LD50) and to reduce testing in animals. *Alternatives to Laboratory Animals, 31*(2), 89-198.

Han, Y. D., Lee, J. W., Park, D. H., Yang, S. H., Kim, B. K., Kim, J., & Joo, J. (2011). Core–shell nanoparticle of silver coated with light-emitting rubrene: Surface plasmon enhanced photoluminescence. *Synthetic Metals, 161*(19), 2103-2106.

Handelman, G. J., Han, D., Tritschler, H., & Packer, L. (1994). Alpha-lipoic acid reduction by mammalian cells to the dithiol form, and release into the culture medium. *Biochemical Pharmacology, 47*(10), 1725-1730.

Hasegawa, H., Fujita, H., Katoh, H., Aoki, J., Nakamura, K., Ichikawa, A., & Negishi, M. (1999). Opposite regulation of transepithelial electrical resistance and paracellular permeability by Rho in Madin-Darby canine kidney cells. *Journal of Biological Chemistry, 274*(30), 20982-20988.

Hu, J., Chen, L., Zhu, K., Suchopar, A., & Richards, R. (2007). Aerobic oxidation of alcohols catalyzed by gold nano-particles confined in the walls of mesoporous silica. *Catalysis Today, 122*(3), 277-283.

Hua, S., To, W. Y., Nguyen, T. T., Wong, M. L., & Wang, C. C. (1996). Purification and characterization of proteasomes from Trypanosoma brucei. *Molecular and Biochemical Parasitology, 78*(1-2), 33-46.

Huang, J., Zhang, X., Wang, C., Wang, L., Li, H., Cao, X., . . . Hu, J. (2008). Size and surface effect of gold nanoparticles (AuNPs)in nanogold-assisted PCR. *Surface Review and Letters, 15*(06), 757-762.

Huang, X., El-Sayed, I. H., Qian, W., & El-Sayed, M. A. (2006). Cancer cell imaging and photothermal therapy in the near-infrared region by using gold nanorods. *Journal of the American Chemical Society, 128*(6), 2115-2120.

Ikuta, N., Tanaka, A., Otsubo, A., Ogawa, N., Yamamoto, H., Mizukami, T., . . . Matsugo, S. (2014). Spectroscopic studies of R(+)-α-lipoic acid—cyclodextrin complexes. *International Journal of Molecular Sciences, 15*, 20469-20485.

Jana, N. R., Gearheart, L., & Murphy, C. J. (2001). Seeding growth for size control of 5−40 nm diameter gold nanoparticles. *Langmuir, 17*(22), 6782-6786.

Jeevanandam, J., Barhoum, A., Chan, Y. S., Dufresne, A., & Danquah, M. K. (2018). Review on nanoparticles and nanostructured materials: History, sources, toxicity and regulations. *Beilstein Journal of Nanotechnology, 9*, 1050-1074.

Jiang, W., Kim, B. Y., Rutka, J. T., & Chan, W. C. (2008). Nanoparticle-mediated cellular response is size-dependent. *Nature Nanotechnology, 3*(3), 145-150.

Joseph, E., & Singhvi, G. (2019). Chapter 4 - Multifunctional nanocrystals for cancer therapy: a potential nanocarrier. In A. M. Grumezescu (Ed.), *Nanomaterials for Drug Delivery and Therapy* (pp. 91-116): William Andrew Publishing.

Kalimuthu, P., & John, S. A. (2010). Studies on ligand exchange reaction of functionalized mercaptothiadiazole compounds onto citrate capped gold nanoparticles. *Materials Chemistry and Physics, 122*(2), 380-385.

Kang, J., Liu, Y., Xie, M. X., Li, S., Jiang, M., & Wang, Y. D. (2004). Interactions of human serum albumin with chlorogenic acid and ferulic acid. *Biochimica et Biophysica Acta, 1674*(2), 205-214.

Kataby, G., Cojocaru, M., Prozorov, R., & Gedanken, A. (1999). Coating carboxylic acids on amorphous iron nanoparticles. *Langmuir, 15*(5), 1703-1708.

Katsuki, T. (1996). Mn-salen catalyst, competitor of enzymes, for asymmetric epoxidation. *Journal of Molecular Catalysis A: Chemical, 113*(1), 87-107.

Khan, J. A., Pillai, B., Das, T. K., Singh, Y., & Maiti, S. (2007). Molecular effects of uptake of gold nanoparticles in HeLa cells. *Chembiochem, 8*(11), 1237-1240.

Khan, T., Vaidya, S., Mhatre, D. S., & Datta, A. (2016). The prospect of salophen in fluorescence lifetime sensing of Al3+. *The Journal of Physical Chemistry B, 120*(39), 10319-10326.

Khlebtsov, B. N., & Khlebtsov, N. G. (2011). On the measurement of gold nanoparticle sizes by the dynamic light scattering method. *Colloid Journal, 73*(1), 118-127.

Khlebtsov, N., & Dykman, L. (2011). Biodistribution and toxicity of engineered gold nanoparticles: A review of in vitro and in vivo studies. *Chemical Society Reviews, 40*(3), 1647-1671.

Kim, G. Y., Shim, J., Kang, M. S., & Moon, S. H. (2008). Optimized coverage of gold nanoparticles at tyrosinase electrode for measurement of a pesticide in various water samples. *Journal of Hazardous Materials, 156*(1-3), 141-147.

Kisselev, A. F., Garcia-Calvo, M., Overkleeft, H. S., Peterson, E., Pennington, M. W., Ploegh, H. L., . . . Goldberg, A. L. (2003). The caspase-like sites of proteasomes, their substrate specificity, new inhibitors and substrates, and allosteric interactions with the trypsin-like sites. *Journal of Biological Chemistry, 278*(38), 35869-35877.

Kochuveedu, S. T., & Kim, D. H. (2014). Surface plasmon resonance mediated photoluminescence properties of nanostructured multicomponent fluorophore systems. *Nanoscale, 6*(10), 4966-4984.

Kondon, M., Kim, J., Udawatte, N., & Lee, D. (2008). Origin of size-dependent energy transfer from photoexcited CdSe quantum dots to gold nanoparticles. *The Journal of Physical Chemistry C, 112*(17), 6695-6699.

Kucuksayan, E., Bozkurt, F., Yilmaz, M. T., Sircan-Kucuksayan, A., Hanikoglu, A., & Ozben, T. (2021). A new combination strategy to enhance apoptosis in cancer

cells by using nanoparticles as biocompatible drug delivery carriers. *Scientific Reports, 11*(1), Article#13027.

Kumaraswamy, S., Bergstedt, T., Shi, X., Rininsland, F., Kushon, S., Xia, W., . . . Whitten, D. (2004). Fluorescent-conjugated polymer superquenching facilitates highly sensitive detection of proteases. *Proceedings of the National Academy of Sciences, 101*(20), 7511-7515.

Lange, T. S., Kim, K. K., Singh, R. K., Strongin, R. M., McCourt, C. K., & Brard, L. (2008). Iron(III)-salophene: An organometallic compound with selective cytotoxic and anti-proliferative properties in platinum-resistant ovarian cancer cells. *PLoS ONE, 3*(5), Article#e2303.

Lecarme, L., Prado, E., De Rache, A., Nicolau-Travers, M.-L., Bonnet, R., Heyden, A. V. D., . . . Thomas, F. (2014). Interaction of polycationic Ni(II)-salophen complexes with G-quadruplex DNA. *Inorganic Chemistry, 53*(23), 12519-12531.

Leoni, L., & Dalla Cort, A. (2018). The supramolecular attitude of metal–salophen and metal–salen complexes. *Inorganics, 6*(2), 42. Retrieved from https://www.mdpi.com/2304-6740/6/2/42

Leu, J. G., Chen, S. A., Chen, H. M., Wu, W. M., Hung, C. F., Yao, Y. D., . . . Liang, Y. J. (2012). The effects of gold nanoparticles in wound healing with antioxidant epigallocatechin gallate and α-lipoic acid. *Nanomedicine, 8*(5), 767-775.

Liang, P., Tang, H., Gu, R., Xue, L., Chen, D., Wang, W., . . . Dong, X. (2019). A pH-responsive zinc (II) metalated porphyrin for enhanced photodynamic/photothermal combined cancer therapy. *Science China Materials, 62*(8), 1199-1209.

Ling, X., Chen, X., Riddell, I. A., Tao, W., Wang, J., Hollett, G., . . . Wu, J. (2018). Glutathione-scavenging poly(disulfide amide) nanoparticles for the effective delivery of Pt(IV) prodrugs and reversal of cisplatin resistance. *Nano Letters, 18*(7), 4618-4625.

Lipsky, M. S., & Sharp, L. K. (2001). From idea to market: The drug approval process. *The Journal of the American Board of Family Practice, 14*(5), 362. Retrieved from http://www.jabfm.org/content/14/5/362.abstract

Liu, Z. X., Robinson, G. B., & Gregory, E. M. (1994). Preparation and characterization of Mn-salophen complex with superoxide scavenging activity. *Archives of Biochemistry and Biophysics, 315*(1), 74-81.

Lu, Z. X., Cui, T., & Shi, Q. L. (1987). Applications of circular dichroism and optical rotatory dispersion in molecular biology. Beijing: Science Press.

Lynch, I., & Dawson, K. A. (2008). Protein-nanoparticle interactions. *Nano Today, 3*(1), 40-47.

Maeda, T., Takeuchi, T., Furusho, Y., & Takata, T. (2004). Design and synthesis of chiral poly(binaphthyl salen zinc complex) and application of the asymmetric field

based on its helical conformation to a catalytic asymmetric reaction. *Journal of Polymer Science Part A: Polymer Chemistry, 42*(18), 4693-4703.

Maheshwari, N., Kumar Atneriya, U., Tekade, M., Sharma, M. C., Elhissi, A., & Tekade, R. K. (2019). Chapter 3 - Guiding Factors and Surface Modification Strategies for Biomaterials in Pharmaceutical Product Development. In R. K. Tekade (Ed.), *Biomaterials and Bionanotechnology* (pp. 57-87): Academic Press.

Maier, S. A. (2007). *Plasmonics: Fundamentals and Applications.*New York: Springer.

Matlou, G. G., Oluwole, D. O., Prinsloo, E., & Nyokong, T. (2018). Photodynamic therapy activity of zinc phthalocyanine linked to folic acid and magnetic nanoparticles. *Journal of Photochemistry and Photobiology B: Biology, 186*, 216-224.

Mendes, R., Fernandes, A. R., & Baptista, P. V. (2017). Gold nanoparticle approach to the selective delivery of gene silencing in cancer-the case for combined delivery? *Genes, 8*(3), Article#94.

Mendes, R. A., Germino, J. C., Fazolo, B. R., Thaines, E. H. N. S., Ferraro, F., Santana, A. M., . . . Barboza, C. A. (2018). Electronic and magnetic properties of the [Ni(salophen)]: An experimental and DFT study. *Journal of Advanced Research, 9*, 27-33.

Michnik, A., Michalik, K., Kluczewska, A., & Drzazga, Z. (2006). Comparative DSC study of human and bovine serum albumin. *Journal of Thermal Analysis and Calorimetry, 84*(1), 113-117.

Miller, J. N. (1983). Photoluminescence and chemiluminescence methods of drug analysis. *Journal of Pharmaceutical and Biomedical Analysis, 1*(4), 525-535.

Min, Y., Mao, C., Xu, D., Wang, J., & Liu, Y. (2010). Gold nanorods for platinum based prodrug delivery. *Chemical Communications, 46*(44), 8424-8426.

Mioc, M., Pavel, I. Z., Ghiulai, R., Coricovac, D. E., Farcaş, C., Mihali, C.-V., . . . Şoica, C. (2018). The cytotoxic effects of betulin-conjugated gold nanoparticles as stable formulations in normal and melanoma cells. *Frontiers in Pharmacology, 9*(429).

Mirabella, Anne C., Pletnev, Alexandre A., Downey, Sondra L., Florea, Bogdan I., Shabaneh, Tamer B., Britton, M., . . . Kisselev, Alexei F. (2011). Specific cell-permeable inhibitor of proteasome trypsin-like sites selectively sensitizes myeloma cells to bortezomib and carfilzomib. *Chemistry & Biology, 18*(5), 608-618.

Mironava, T., Hadjiargyrou, M., Simon, M., Jurukovski, V., & Rafailovich, M. H. (2010). Gold nanoparticles cellular toxicity and recovery: Effect of size, concentration and exposure time. *Nanotoxicology, 4*(1), 120-137.

Mirzaei, M., & Pili, H. B. (2015). Potentiometric determination of cadmium using coated platinum and PVC membrane sensors based on N,N'-bis(salicylaldehyde)phenylenediamine (salophen). *Journal of Analytical Chemistry, 70*(6), 731-737.

More, M. S., Pawal, S. B., Lolage, S. R., & Chavan, S. S. (2017). Syntheses, structural characterization, luminescence and optical studies of Ni(II) and Zn(II) complexes containing salophen ligand. *Journal of Molecular Structure, 1128*, 419-427.

Mota, V. Z., de Carvalho, G. S. G., Corbi, P. P., Bergamini, F. R. G., Formiga, A. L. B., Diniz, R., . . . Cuin, A. (2012). Crystal structure and theoretical studies of the keto-enol isomerism of N,N′ -bis(salicylidene)-o-phenylenediamine (salophen). *Spectrochimica Acta Part A: Molecular and Biomolecular Spectroscopy, 99*, 110-115.

Mthethwa, T. P., Tuncel, S., Durmuş, M., & Nyokong, T. (2013). Photophysical and photochemical properties of a novel thiol terminated low symmetry zinc phthalocyanine complex and its gold nanoparticles conjugate. *Dalton Transactions, 42*(14), 4922-4930.

Mucic, R. C., Storhoff, J. J., Mirkin, C. A., & Letsinger, R. L. (1998). DNA-directed synthesis of binary nanoparticle network materials. *Journal of the American Chemical Society, 120*(48), 12674-12675.

Murawala, P., Phadnis, S. M., Bhonde, R. R., & Prasad, B. L. (2009). In situ synthesis of water dispersible bovine serum albumin capped gold and silver nanoparticles and their cytocompatibility studies. *Colloids and Surfaces B, Biointerfaces, 73*(2), 224-228.

Mutua, G. K., Bellam, R., Jaganyi, D., & Mambanda, A. (2019). The role of N,N-chelate ligand on the reactivity of (η6-p-cymene)Ru(II) complexes: Kinetics, DNA and protein interaction studies. *Journal of Coordination Chemistry, 72*(17), 2931-2956.

Navarrete, J., Siefe, C., Alcantar, S., Belt, M., Stucky, G. D., & Moskovits, M. (2018). Merely measuring the UV–visible spectrum of gold nanoparticles can change their charge state. *Nano Letters, 18*(2), 669-674.

Naveenraj, S., Anandan, S., Kathiravan, A., Renganathan, R., & Ashokkumar, M. (2010). The interaction of sonochemically synthesized gold nanoparticles with serum albumins. *Journal of Pharmaceutical and Biomedical Analysis, 53*(3), 804-810.

Ng, C.-H., Wang, W.-S., Chong, K.-V., Win, Y.-F., Neo, K.-E., Lee, H.-B., . . . Leong, W. K. (2013). Ternary copper(ii)-polypyridyl enantiomers: aldol-type condensation, characterization, DNA-binding recognition, BSA-binding and anticancer property. *Dalton Transactions, 42*(28), 10233-10243.

Niidome, T., Yamagata, M., Okamoto, Y., Akiyama, Y., Takahashi, H., Kawano, T., . . . Niidome, Y. (2006). PEG-modified gold nanorods with a stealth character for in vivo applications. *Journal of Controlled Release, 114*(3), 343-347.

Oliveri, I. P., & Di Bella, S. (2011). Sensitive fluorescent detection and Lewis basicity of aliphatic amines. *The Journal of Physical Chemistry A, 115*(50), 14325-14330.

Oliveri, V., & Vecchio, G. (2011). A novel artificial superoxide dismutase: Non-covalent conjugation of albumin with a MnIII salophen type complex. *European Journal of Medicinal Chemistry, 46*(3), 961-965.

Omura, K., Uchida, T., Irie, R., & Katsuki, T. (2004). Design of a robust Ru(salen) complex: aziridination with improved turnover number using N-arylsulfonyl azides as precursors. *Chemical Communications*(18), 2060-2061.

Ouari, K., Bendia, S., Weiss, J., & Bailly, C. (2015). Spectroscopic, crystal structural and electrochemical studies of zinc(II)-Schiff base complex obtained from 2,3-diaminobenzene and 2-hydroxy naphthaldehyde. *Spectrochimica Acta Part A: Molecular and Biomolecular Spectroscopy, 135*, 624-631.

Packer, L., Tritschler, H. J., & Wessel, K. (1997). Neuroprotection by the metabolic antioxidant alpha-lipoic acid. *Free Radical Biology & Medicine, 22*(1-2), 359-378.

Pan, Y., Neuss, S., Leifert, A., Fischler, M., Wen, F., Simon, U., . . . Jahnen-Dechent, W. (2007). Size-dependent cytotoxicity of gold nanoparticles. *Small, 3*(11), 1941-1949.

Parker, J. P., Ude, Z., & Marmion, C. J. (2015). Exploiting developments in nanotechnology for the preferential delivery of platinum-based anti-cancer agents to tumours: targeting some of the hallmarks of cancer. *Metallomics, 8*(1), 43-60.

Patra, J. K., & Baek, K.-H. (2015). Novel green synthesis of gold nanoparticles using Citrullus lanatus rind and investigation of proteasome inhibitory activity, antibacterial, and antioxidant potential. *International Journal of Nanomedicine, 10*, 7253-7264.

Pernodet, N., Fang, X., Sun, Y., Bakhtina, A., Ramakrishnan, A., Sokolov, J., . . . Rafailovich, M. (2006). Adverse effects of citrate/gold nanoparticles on human dermal fibroblasts. *Small, 2*(6), 766-773.

Pitsillides, C. M., Joe, E. K., Wei, X., Anderson, R. R., & Lin, C. P. (2003). Selective cell targeting with light-absorbing microparticles and nanoparticles. *Biophysical Journal, 84*(6), 4023-4032.

Pompa, P. P., Martiradonna, L., Torre, A. D., Sala, F. D., Manna, L., De Vittorio, M., . . . Rinaldi, R. (2006). Metal-enhanced fluorescence of colloidal nanocrystals with nanoscale control. *Nature Nanotechnology, 1*(2), 126-130.

Pramanik, A. K., Siddikuzzaman, Palanimuthu, D., Somasundaram, K., & Samuelson, A. G. (2016). Biotin decorated gold nanoparticles for targeted delivery of a smart-linked anticancer active copper complex: In vitro and in vivo studies. *Bioconjugate Chemistry, 27*(12), 2874-2885.

Rani, J. J., Jayaseeli, A. M. I., Rajagopal, S., Seenithurai, S., Chai, J.-D., Raja, J. D., & Rajasekaran, R. (2021). Synthesis, characterization, antimicrobial, BSA binding, DFT calculation, molecular docking and cytotoxicity of Ni(II) complexes with Schiff base ligands. *Journal of Molecular Liquids, 328*, 115457.

Redza-Dutordoir, M., & Averill-Bates, D. A. (2016). Activation of apoptosis signalling pathways by reactive oxygen species. *Biochimica et Biophysica Acta – Molecular Cell Research, 1863*(12), 2977-2992.

Reetz, M. T., & Helbig, W. (1994). Size-selective synthesis of nanostructured transition metal clusters. *Journal of the American Chemical Society, 116*(16), 7401-7402.

Reineck, P., Gómez, D., Ng, S. H., Karg, M., Bell, T., Mulvaney, P., & Bach, U. (2013). Distance and wavelength dependent quenching of molecular fluorescence by Au@SiO2 core–shell nanoparticles. *ACS Nano, 7*(8), 6636-6648.

Rogers, D. M., Jasim, S. B., Dyer, N. T., Auvray, F., Réfrégiers, M., & Hirst, J. D. (2019). Electronic circular dichroism spectroscopy of proteins. *Chem, 5*(11), 2751-2774.

Rogers, N. J., Claire, S., Harris, R. M., Farabi, S., Zikeli, G., Styles, I. B., . . . Pikramenou, Z. (2014). High coating of Ru(ii) complexes on gold nanoparticles for single particle luminescence imaging in cells. *Chemical Communications, 50*(5), 617-619.

Rosenthal-Kim, E. Q. (2013). *Green Polymer Chemistry: Synthesis of Poly(disulfide) Polymers and Networks.* (Doctoral dissertation). University of Akron, Ohio, United States.

Routier, S., Vezin, H., Lamour, E., Bernier, J. L., Catteau, J. P., & Bailly, C. (1999). DNA cleavage by hydroxy-salicylidene-ethylendiamine-iron complexes. *Nucleic Acids Research, 27*(21), 4160-4166.

Saito, G., Swanson, J. A., & Lee, K.-D. (2003). Drug delivery strategy utilizing conjugation via reversible disulfide linkages: Role and site of cellular reducing activities. *Advanced Drug Delivery Reviews, 55*(2), 199-215.

Salmaso, S., Caliceti, P., Amendola, V., Meneghetti, M., Magnusson, J. P., Pasparakis, G., & Alexander, C. (2009). Cell up-take control of gold nanoparticles functionalized with a thermoresponsive polymer. *Journal of Materials Chemistry, 19*(11), 1608-1615.

Sandoval, J., Ventura-Sobrevilla, J., Boone-Villa, D., Ramos-González, R., Velázquez, M., Silva-Belmares, Y., . . . Aguilar, C. (2019). Chapter 14 - Carbon nanomaterials as pharmaceutic forms for sustained and controlled delivery systems. In A. M. Grumezescu (Ed.), *Nanomaterials for Drug Delivery and Therapy* (pp. 403-434): William Andrew Publishing.

Satake, A., Fujita, M., Kurimoto, Y., & Kobuke, Y. (2009). Single supramolecular porphyrin wires bridging gold nanoparticles. *Chemical Communications*(10), 1231-1233.

Schaeublin, N. M., Braydich-Stolle, L. K., Schrand, A. M., Miller, J. M., Hutchison, J., Schlager, J. J., & Hussain, S. M. (2011). Surface charge of gold nanoparticles mediates mechanism of toxicity. *Nanoscale, 3*(2), 410-420.

Sergeev, G. B., & Klabunde, K. J. (2013). Chapter 4 - Experimental Techniques. In G. B. Sergeev & K. J. Klabunde (Eds.), *Nanochemistry (Second Edition)* (pp. 75-87). Oxford: Elsevier.

Shaghaghi, Z., Kalantari, N., Kheyrollahpoor, M., & Haeili, M. (2020). Optical, electrochemical, thermal, biological and theoretical studies of some chloro and

bromo based metal-salophen complexes. *Journal of Molecular Structure, 1200*, Article#127107.

Shaikh, S. M. T., Seetharamappa, J., Kandagal, P. B., Manjunatha, D. H., & Ashoka, S. (2007). Spectroscopic investigations on the mechanism of interaction of bioactive dye with bovine serum albumin. *Dyes and Pigments, 74*(3), 665-671.

Shang, L., Wang, Y., Jiang, J., & Dong, S. (2007). pH-dependent protein conformational changes in albumin: Gold nanoparticle bioconjugates: A spectroscopic study. *Langmuir, 23*(5), 2714-2721.

Shankar, S. S., Rai, A., Ankamwar, B., Singh, A., Ahmad, A., & Sastry, M. (2004). Biological synthesis of triangular gold nanoprisms. *Nature Materials, 3*(7), 482-488.

Shi, J.-h., Pan, D.-q., Jiang, M., Liu, T.-T., & Wang, Q. (2016). Binding interaction of ramipril with bovine serum albumin (BSA): Insights from multi-spectroscopy and molecular docking methods. *Journal of Photochemistry and Photobiology B: Biology, 164*, 103-111.

Shi, X., Li, D., Xie, J., Wang, S., Wu, Z., & Chen, H. (2012). Spectroscopic investigation of the interactions between gold nanoparticles and bovine serum albumin. *Chinese Science Bulletin, 57*(10), 1109-1115.

Siew, A., Le, H., Thiovolet, M., Gellert, P., Schatzlein, A., & Uchegbu, I. (2012). Enhanced oral absorption of hydrophobic and hydrophilic drugs using quaternary ammonium palmitoyl glycol chitosan nanoparticles. *Molecular Pharmaceutics, 9*(1), 14-28.

Slepička, P., Slepičková Kasálková, N., Siegel, J., Kolská, Z., & Švorčík, V. (2019). Methods of gold and silver nanoparticles preparation. *Materials (Basel, Switzerland), 13*(1), Article#1.

Sood, D., Kumar, N., Rathee, G., Singh, A., Tomar, V., & Chandra, R. (2018). Mechanistic interaction study of bromo-noscapine with bovine serum albumin employing spectroscopic and chemoinformatics approaches. *Scientific Reports, 8*(1), Article#16964.

Srinivasan, B., Kolli, A. R., Esch, M. B., Abaci, H. E., Shuler, M. L., & Hickman, J. J. (2015). TEER measurement techniques for in vitro barrier model systems. *Journal of Laboratory Automation, 20*(2), 107-126.

Sujitha, M. V., & Kannan, S. (2013). Green synthesis of gold nanoparticles using Citrus fruits (Citrus limon, Citrus reticulata and Citrus sinensis) aqueous extract and its characterization. *Spectrochimica Acta Part A: Molecular and Biomolecular Spectroscopy, 102*, 15-23.

Sułkowska, A. (2002). Interaction of drugs with bovine and human serum albumin. *Journal of Molecular Structure, 614*(1), 227-232.

Suryawanshi, V. D., Walekar, L. S., Gore, A. H., Anbhule, P. V., & Kolekar, G. B. (2016). Spectroscopic analysis on the binding interaction of biologically active

pyrimidine derivative with bovine serum albumin. *Journal of Pharmaceutical Analysis, 6*(1), 56-63.

Tsoli, M., Kuhn, H., Brandau, W., Esche, H., & Schmid, G. (2005). Cellular uptake and toxicity of Au55 clusters. *Small, 1*(8-9), 841-844.

Turkevich, J., Stevenson, P. C., & Hillier, J. (1951). A study of the nucleation and growth processes in the synthesis of colloidal gold. *Discussions of the Faraday Society, 11*(0), 55-75.

Tverdova, N. V., Giricheva, N. I., Girichev, G. V., Kuz'mina, N. P., Kotova, O. V., & Zakharov, A. V. (2009). IR spectra of N,N'-ethylene-bis(salicylaldiminates) and N,N'-ethylene-bis(acetylacetoniminates) of Ni(II), Cu(II), and Zn(II). *Russian Journal of Physical Chemistry A, 83*(13), 2255-2265.

Valko, M., Izakovic, M., Mazur, M., Rhodes, C. J., & Telser, J. (2004). Role of oxygen radicals in DNA damage and cancer incidence. *Molecular and Cellular Biochemistry, 266*(1-2), 37-56.

Venkataramanan, N. S., Kuppuraj, G., & Rajagopal, S. (2005). Metal-salen complexes as efficient catalysts for the oxygenation of heteroatom containing organic compounds-synthetic and mechanistic aspects. *Coordination Chemistry Reviews, 249*(11), 1249-1268.

Vigderman, L., & Zubarev, E. R. (2013). Therapeutic platforms based on gold nanoparticles and their covalent conjugates with drug molecules. *Advanced Drug Delivery Reviews, 65*(5), 663-676.

Villiers, C., Freitas, H., Couderc, R., Villiers, M. B., & Marche, P. (2010). Analysis of the toxicity of gold nano particles on the immune system: effect on dendritic cell functions. *Journal of Nanoparticle Research, 12*(1), 55-60.

Vitale, F., Vitaliano, R., Battocchio, C., Fratoddi, I., Piscopiello, E., Tapfer, L., & Russo, M. V. (2008). Synthesis and characterization of gold nanoparticles stabilized by palladium(II) phosphine thiol. *Journal of Organometallic Chemistry, 693*(6), 1043-1048.

Vuignier, K., Schappler, J., Veuthey, J. L., Carrupt, P. A., & Martel, S. (2010). Drug-protein binding: A critical review of analytical tools. *Analytical and Bioanalytical Chemistry, 398*(1), 53-66.

Wagner, S., Kufleitner, J., Zensi, A., Dadparvar, M., Wien, S., Bungert, J., . . . Briesen, H. V. (2010). Nanoparticulate transport of oximes over an in vitro blood-brain barrier model. *PLoS ONE, 5*(12), Article#e14213.

Wang, M., Wang, L., Wang, G., Ji, X., Bai, Y., Li, T., . . . Li, J. (2004). Application of impedance spectroscopy for monitoring colloid Au-enhanced antibody immobilization and antibody-antigen reactions. *Biosens Bioelectron, 19*(6), 575-582.

Wu, P., Ma, D.-L., Leung, C.-H., Yan, S.-C., Zhu, N., Abagyan, R., & Che, C.-M. (2009). Stabilization of G-quadruplex DNA with platinum(II) Schiff base complexes:

Luminescent probe and down-regulation of c-myc oncogene expression. *Chemistry – A European Journal, 15*(47), 13008-13021.

Yah, C. (2013). The toxicity of gold nanoparticles in relation to their physiochemical properties. *Biomedical Research, 24*, 400-413.

Yeh, C.-M., Chen, M.-C., Wu, T.-C., Chen, J.-W., & Lai, C.-H. (2021). Lectin-triggered aggregation of glyco-gold nanoprobes for activity-based sensing of hydrogen peroxide by the naked eye. *Chemistry – An Asian Journal, 16*(21), 3462-3468.

Young, A. G., Green, D. P., & McQuillan, A. J. (2007). IR spectroscopic studies of adsorption of dithiol-containing ligands on CdS nanocrystal films in aqueous solutions. *Langmuir, 23*(26), 12923-12931.

Yuan, K., Qin, R., Yu, J., Li, X., Li, L., Yang, X., . . . Liu, H. (2020). Effects of localized surface plasmon resonance of Ag nanoparticles on luminescence of carbon dots with blue, green and yellow emission. *Applied Surface Science, 502*, Article#144277.

Zhang, H., Hussain, I., Brust, M., & Cooper, A. I. (2004). Emulsion-templated gold beads using gold nanoparticles as building blocks. *Advanced Materials, 16*(1), 27-30.

Zhang, P., Wang, J., Huang, H., Qiu, K., Huang, J., Ji, L., & Chao, H. (2017). Enhancing the photothermal stability and photothermal efficacy of AuNRs and AuNTs by grafting with Ru(ii) complexes. *Journal of Materials Chemistry B, 5*(4), 671-678.

Zhang, P., Wang, J., Huang, H., Yu, B., Qiu, K., Huang, J., . . . Chao, H. (2015). Unexpected high photothemal conversion efficiency of gold nanospheres upon grafting with two-photon luminescent ruthenium(II) complexes: A way towards cancer therapy? *Biomaterials, 63*, 102-114.

Zhang, X.-Q., Xu, X., Lam, R., Giljohann, D., Ho, D., & Mirkin, C. A. (2011). Strategy for increasing drug solubility and efficacy through covalent attachment to polyvalent DNA–nanoparticle conjugates. *ACS Nano, 5*(9), 6962-6970.

Zhang, Y., Xu, D., Li, W., Yu, J., & Chen, Y. (2012). Effect of size, shape, and surface modification on cytotoxicity of gold nanoparticles to human HEp-2 and canine MDCK Cells. *Journal of Nanomaterials, 2012*, Article#375496.

Zhu, C., Hu, W., Wu, H., & Hu, X. (2014). No evident dose-response relationship between cellular ROS level and its cytotoxicity - a paradoxical issue in ROS-based cancer therapy. *Scientific Reports, 4*(1), Article#5029.

Zhuo, Y., Yuan, R., Chai, Y., Tang, D., Zhang, Y., Wang, N., . . . Zhu, Q. (2005). A reagentless amperometric immunosensor based on gold nanoparticles/thionine/Nafion-membrane-modified gold electrode for determination of α-1-fetoprotein. *Electrochemistry Communications, 7*(4), 355-360.